

Article

Not peer-reviewed version

---

# Geochemical Characteristics of Modern River-Sand and Its Bearing on the Mineral Exploration in the Manufahi Area, Timor-Leste

---

[Vital Vilanova](#)\*, [Tomoyuki Ohtani](#)\*, [Satoru Kojima](#), [Kazuma Yatabe](#), [Elizario Moniz](#)

Posted Date: 23 August 2024

doi: 10.20944/preprints202408.1641.v1

Keywords: Manufahi area; Timor-Leste; river sands; X-ray fluorescence (XRF) analysis; geochemical anomaly; statistical analysis; mineralization; mineral exploration



Preprints.org is a free multidiscipline platform providing preprint service that is dedicated to making early versions of research outputs permanently available and citable. Preprints posted at Preprints.org appear in Web of Science, Crossref, Google Scholar, Scilit, Europe PMC.

Copyright: This is an open access article distributed under the Creative Commons Attribution License which permits unrestricted use, distribution, and reproduction in any medium, provided the original work is properly cited.

Article

# Geochemical Characteristics of Modern River-Sand and Its Bearing on the Mineral Exploration in the Manufahi Area, Timor-Leste

Vital Vilanova<sup>1,2,\*</sup>, Tomoyuki Ohtani<sup>1,\*</sup>, Satoru Kojima<sup>1</sup>, Kazuma Yatabe<sup>1</sup> and Elizario Moniz<sup>3</sup>

<sup>1</sup> Department of Civil Engineering, Gifu University, 1-1 Yanagido, Gifu 501-1193, Japan; kojima.satoru.r6@f.gifu-u.ac.jp (S.K.); basketman.mero7@gmail.com (K.Y.)

<sup>2</sup> Department of Geology and Petroleum Engineering, National University of Timor Lorosa'e, Dili, Timor-Leste

<sup>3</sup> Instituto de Geociência de Timor-Leste, Dili, Timor-Leste; milagrosa.xaviera@gmail.com (E.M.)

\* Correspondence: araujo.vilanova.vital.cruz.malai.b2@s.gifu-u.ac.jp (V.V.); ohtani.tomoyuki.g9@f.gifu-u.ac.jp (T.O.)

**Abstract:** Geochemical mapping of river sands in the Manufahi area of Timor-Leste revealed potential areas for future mineral exploration. River sand samples from the study area were collected and geochemically analyzed to identify anomalous concentration distributions of several valuable elements and locate potential target areas and geological formations that may host mineral deposits. The 26 major and minor elements were identified using wavelength-dispersive X-ray fluorescence. The river sands exhibited varying elemental concentrations, with Cr, Cu, Zn, and Ba showing deviations from the normal distribution patterns. Identification of geochemical anomalies is an important task in mineral exploration geochemistry. The mean + 2 standard deviations (mean+2STD), median + 2 median absolute deviations (median+2MAD), and Tukey's inner fence (TIF) methods were used to determine the geochemical thresholds. This study shows that TIF and principal component analysis (PCA) methods are highly effective in calculating appropriate threshold values and identifying relevant elemental associations. These approaches have proven useful for delineating target areas for mineral deposits, resulting in reliable outcomes. Four predicted target areas with high potential for deposits and mineralization anomalies of Cr, Cu, Ni, and Ba were delineated in the study area.

**Keywords:** Manufahi area; Timor-Leste; river sands; X-ray fluorescence (XRF) analysis; geochemical anomaly; statistical analysis; mineralization; mineral exploration.

## 1. Introduction

"River sand" is the term used to refer to the samples under analysis in this study [1–3]. Fine-to-coarse sand fractions were obtained from the active channel below the water level. Modern river sand is an effective medium for geochemical mapping in many regions worldwide including Japan [4,5], Portugal [6], Brazil [7], and Australia [8]. The characteristics of modern river sands in drainage basins are often influenced by various factors, including source rock lithologies, mineral deposit occurrence, climate, topographic relief, transportation, and depositional environment [8–10]. However, the source area materials appear to have the greatest influence on the geochemistry of modern river sands [11–15]. Geochemical data for river sand and other surface sediments often deviate from a normal distribution [16]. The potential occurrence of mineral deposits or atypical lithologies, such as iron-rich sedimentary rocks, radiolarian cherts, carbonatites, and serpentinites, may be responsible for the high elemental concentrations found in river sands [17].

The main duty of the geochemical assessment of mineral resource prospects in the identification of potential areas for further investigation is to determine and separate anomalies, thresholds, and background values [18,19]. Various statistical analyses and methods have been employed using different approaches and parameters, including univariate, bivariate, multivariate, and spatial analyses. These include mean, median, mode, standard deviation, variance, skewness, kurtosis, median absolute deviation (MAD), interquartile range (IQR), Tukey's inner fence (TIF), mean + 2 standard deviations (mean+2STD), median + 2 median absolute deviations (median+2MAD), and an association of distribution plots, such as histograms, boxplots, and normal quantile plots, to characterize anomalies and

define threshold and background values in a univariate data set that falls outside a normal distribution. Additionally, the Spearman correlation coefficient, principal component analysis (PCA), and inverse distance weighting (IDW) interpolation methods were applied to identify the original geochemical signatures of the source composition and the distribution of anomalies that may be related to mineral deposits or atypical lithologies [19–27].

In 1936, mineral exploration was conducted in the research area by the Allied Mining Corporation, resulting in the discovery of several potential mineralization areas [28]. Subsequent studies and research projects have been conducted, providing information on the occurrence of massif sulfide mineralization and other mineral deposits in the area, including those by Leme [29], Lacerda [30], and ESCAP [31]. However, geochemical mapping investigations were not conducted or documented in these reports.

This study focused on the geochemistry of river sands with the main objective of gathering important information regarding the anomalous concentration distributions of valuable elements and identifying potential target areas and geological formations that may host mineral deposits in the study area. The results of this study can serve as a basis and provide useful information for future geochemical mapping and mineral exploration campaigns in Timor-Leste and similar global geological settings.

## 2. Geographical and Geological Setting

The territory of Timor-Leste comprises the eastern portion of the island of Timor, the small offshore areas of Atauro Island and Jaco Islet, and the enclave of Oecusse (Figure 1). Geologically, the small island of Atauro is part of the inner Banda arc of the volcanic island. Timor and Jaco Islet are part of the outer Banda arcs and are non-volcanic islands formed by orogenic processes resulting from the collision between the passive margin of the Australian continent and the Banda volcanic arc of the Eurasian plate after the subduction of the Indian Ocean crust [32–37]. The study area is geographically located on the south coast of Timor-Leste, approximately 100 km south of the capital city, Dili. The study area is largely characterized by rugged to moderate mountainous topography, with various slopes ranging from moderate to steep.

As delineated by Audley-Charles [38], Bachri and Situmorang [39], and Partoyo et al. [40], along with geological research and mapping carried out by other researchers [36,41–51], the study area encompasses several formations (Figure 1C): (a) Suai Formation, is Pleistocene to the Holocene in age and predominantly consists of rudites and arenites, with minor proportions of mud and marls; (b) Ainaro Formation is Pleistocene to Holocene in age and primarily consists of matrix-supported conglomerates; (c) Baucau Limestone, which ranges in age from the Lower Pleistocene to the Holocene, primarily consists of coral-reef limestones, along with minor amounts of calcarenites, calcirudites, and conglomerates; (d) Dilor Conglomerate, composed of sandstones and conglomerates with significant detritus input from the quartzites of the Lolotoi Complex, is Pliocene in age; (e) Viqueque Formation, dating from the Upper Miocene to the Lower Pliocene, is lithologically divided into two sections: (i) the upper layer comprises significant proportions of silty marls, marly siltstones, silty claystones, siltstones, and sandstones, as well as lesser calcilutites and biocalcarenes; (ii) the lower layer contains minor proportions of basal conglomerates and mottled marls, along with notable amounts of marls, clayey marls, silty marls, calcilutites, and tuffs; (f) Bobonaro Complex, Middle Miocene in age, is dominated by exotic blocks within a scaly clay matrix. The matrix lithology resembles that of the mudstone of the Wailuli Formation.

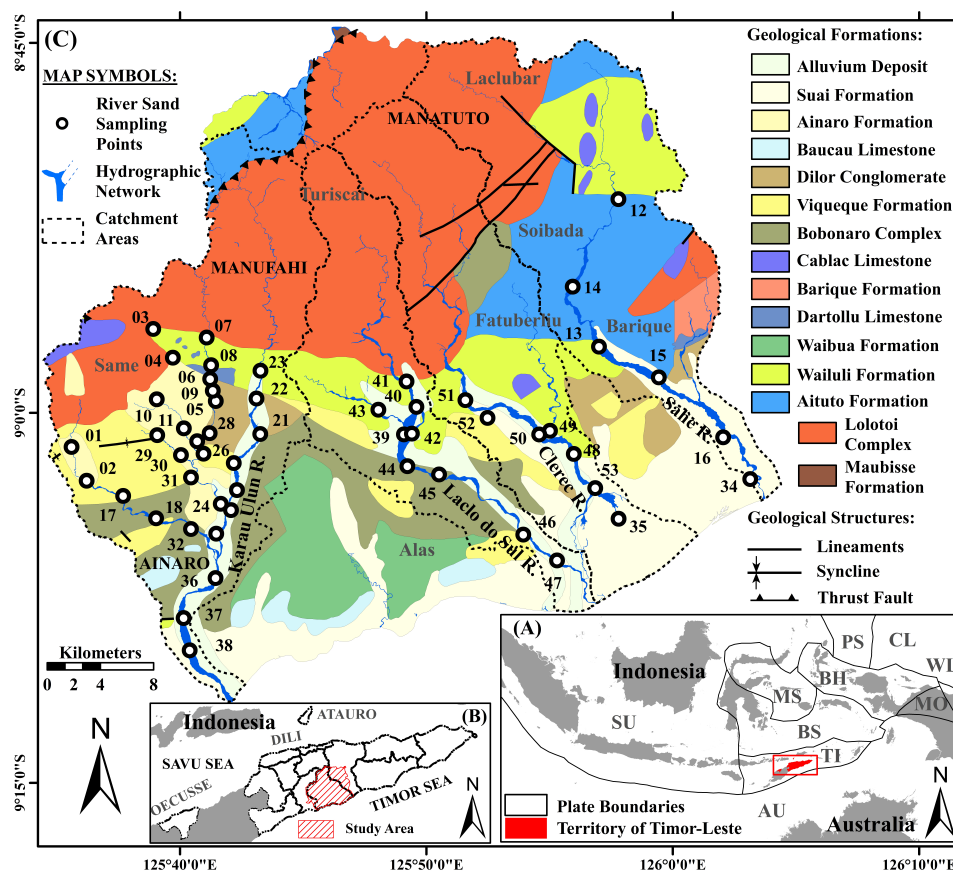


**Figure 1.** (A) Geographic map of Timor-Leste and the plate tectonic boundaries of Southeast Asia. Bold greyish-black lines are used to delineate the borders of the Sunda (SU), Australia (AU), Timor (TI), Banda Sea (BS), Molucca Sea (MS), Bird's Head (BH), Philippine Sea (PS), Caroline (CL), Woodlark (WL), and Maoke (MO) plates (adapted from Bird [52], Pistu [53], Poiata et al. [54]). (B) The geographical location of the study area and its surroundings. The municipalities of Timor-Leste are delineated by heavy black lines (adapted from Pistu [53]). (C) Geological formation map and the distribution of river-sand sampling points in the study area (adapted from Bachri and Situmorang [39], Partoyo et al. [40]).

Exotic blocks that are Permian to Cretaceous in ages are common and extensively distributed; (g) Cablac Limestone, ranging in age from the Oligocene to the Miocene, predominantly consists of oolitic and peloidal limestones, pelagic carbonates, and minor proportions of intraformational conglomerates, calcilutites, calcarenites, agglomerates, and tuffaceous rocks; (h) Barique Formation is Oligocene in age and is primarily composed of mafic to acidic lavas and tuffs, with lesser amounts of serpentinites, volcanic conglomerates, and sandstones; (i) Dartollu Limestone, which has been dated to the Middle–Upper Eocene, is largely composed of algal and alveolina biomicarenites, with minor amounts of calcilutites, siliceous shales, and siltstones; (j) Waibua Formation ranges in age from the Lower to the Upper Cretaceous and mainly consists of radiolarites, radiolarian cherts, marls, and shales, with varying proportions of calcilutites, marls, and calcarenites; (k) Wailuli Formation, in which the major constituents include gray shales and blue-gray marls, with lesser amounts of sandstones, mudstones, quartz-arenites, coarse polymictic conglomerates, calcarenites, and calcilutites, is Late Triassic to Middle Jurassic in age. Most shales are characterized by fine micaceous minerals and microcrystalline carbonates, with small amounts of pyrite; (l) Aitutu Formation, which ranges in age from the Middle to Upper Triassic, is largely composed of calcilutites, shales, and calcareous shales with minor proportions of marls, calcarenites, lumachelles, quartz-arenites, radiolarites, bituminous rocks, and cherts. Several limestones have undergone silicification, dedolomitization, and pyritization

processes; (m) Lolotoi Complex mainly consist of regional metasedimentary and metavolcanic rocks, along with basic and ultrabasic volcanic rocks. Most metamorphic rocks within the Lolotoi Complex are derived from sedimentary rocks. This formation dates from the Triassic to the Late Cretaceous; and (n) Maubisse Formation, which is Permian in age, largely comprises fossiliferous limestones and volcanic rocks, along with well-bedded dense biocalcarenites, massive reef limestones, pink crinoidal limestones, calcirudites, sandstones, calcareous shales, micaceous siltstones, tuffs, volcanic conglomerates, basalts, marbles, and metamorphosed basic volcanics.

### 3. Samples and Methods

#### 3.1. Sampling and Preparation

In this study, basic procedures for sampling river sand and treating samples before chemical analysis, as outlined in Hale and Plant [55], Darnley et al. [56], Tanaka et al. [57], Fletcher [58], Ohta et al. [59], and Yamamoto et al. [5], were implemented. Modern river sand samples were collected from 53 sites in the study area (Figure 1). Samples were dried in an oven at 105 °C and then sieved using a vibrating sieve shaker machine. The composite samples of fine-grained river sands sieved through 180–150 and < 150  $\mu\text{m}$  metal sieves were ground using an agate mortar and pestle, followed by machine crushing using an agate ball mill. Organic matter and volatile compounds in the samples were removed using the loss-on-ignition method, and it was determined by measuring the weight loss after heating to 950 °C.

As described and recommended by Yamamoto and Morishita [60], to analyze major and minor elements, glass beads were used for sample preparation in X-ray fluorescence (XRF) analysis. The fused glass beads were prepared by mixing the powder at a sample-to-flux ratio of one to two after heating. The flux used was a crystalline powder of anhydrous lithium tetraborate ( $\text{Li}_2\text{B}_4\text{O}_7 = 169.12$ ). The mixed powder was placed in a platinum crucible and processed using a bead sampler (TK-4100 model, Amena Tech Co., Yokohama, Japan) to form glass beads.

#### 3.2. Analytical Methods and Data Analysis

Fifty-three modern river sand samples were analyzed using wavelength-dispersive XRF (WD-XRF) at the Division of Instrumental Analysis, Gifu University, and 26 major and minor element concentrations were determined. These elements were accurately calibrated using standard reference samples provided by the Geological Survey of Japan (GSJ).

##### 3.2.1. Univariate Analysis

In this study, basic and classical descriptive statistics refer to univariate analyses, which include the calculation and estimation of minimum, maximum, mean, mode, median, variance, range, standard deviation, and quartile values. In addition to the aforementioned parameters, skewness and kurtosis were employed as initial estimates to indicate the distribution characteristics of the studied geochemical elements. In normal distributions, the skewness is zero and the kurtosis is approximately three, whereas the mean, mode, and median values are nearly identical [61–64]. In addition, statistical methods such as mean+2STD, median+2MAD, and TIF are the most precise methods for defining anomaly threshold values. In certain cases, where the raw geochemical data did not follow a normal distribution, the mean+2STD method failed to provide a relevant threshold estimate. The TIF method was calculated using the formula:  $[\text{TIF} = \text{Q}_3 + 1.5 \times \text{IQR}]$ , where the third quartile ( $\text{Q}_3$ ) represents the 75th percentile value ( $\text{Q}_{75}$ ), and interquartile range (IQR) represents the difference between the 75th and 25th percentile values ( $\text{Q}_3 - \text{Q}_1$ ) [19,20,22,65–68].

The distribution plots, which involve the joint application of several graphs and diagrams, such as normal quantile plots, boxplots, and histograms, are focused on visualizing, simplifying, and clarifying the distribution and characteristics, or any deviations, in the studied geochemical elements that could be attributed to the contributions of the underlying lithologies or mineral deposits [64,69–71]. The

elements of the boxplot (Figure 2) reveal that the box represents the hinge width or IQR, which is defined as the absolute difference between the third and first quartile values. The second quartile (median) is marked by a line within the box. The lower and upper "inner fences" and "outer fences" were drawn at 1.5 and 3 times the hinge width, extending towards the lowest and highest values, respectively. The boxplot categorizes a set of geochemical element data into five reliable classes as follows [69]: (a) the lowest-lower whisker is classified as extremely low background; (b) lower whisker-lower hinge is labelled as low background; (c) lower hinge-upper hinge is defined as background; (d) upper hinge-upper whisker is considered high background; and (e) upper whisker-highest is classified as an anomaly. In addition, the upper inner fence was defined as the threshold for separating the background from anomalous values.



Figure 2. Schematic features of a boxplot.

### 3.2.2. Bivariate and Multivariate Analyses

The Spearman correlation coefficient was employed to identify and evaluate the inter-relationships between the variables of the geochemical elements that deviated from a normal distribution [72]. PCA is one of the most commonly used techniques for multivariate statistical analyses and is an effective and reliable approach for extracting information and determining the composition of geochemical populations [9,23,73], outlining the source composition of underlying lithologies and identifying areas of interest for the potential occurrence of mineral deposits [27,74]. Only principal components with eigenvalues greater than or near 1.0 were used to analyze and interpret PCA results in a biplot of joint graphical representations of variables and samples because they represent most of the variance in the data [66,75,76]. IDW is a deterministic, predictable, and reproducible approach for multivariate spatial techniques that can be applied to compute and interpolate values in areas where samples were not collected. IDW assigns more influence on the interpolated value to the points closest to the known value points than to those farther away [77]. In this study, IDW was employed to create a surface model that represented the spatial distribution of multi-element associations derived from the PCA scores along with several independent variables.

Descriptive statistics, distribution plots, Spearman's correlation coefficients, and PCA were performed using Microsoft Office Excel version 2405 (Build 17628.20144) and JMP Pro 14. Additionally, the maps presented in this study, including interpolated and geological maps, were created using ArcGIS 10.4.

## 4. Results

### 4.1. Statistical and Distribution Characteristics of Geochemical Elements

The basic and classical descriptive statistics of the univariate analysis of the 26 raw geochemical elements in river sands from the study area are summarized in Table 1. In this study, we present geochemical analysis results for both major and minor elements. However, our focus was on minor elements, as the geochemical characteristics of the major elements regarding their provenance have already been discussed and published [78].

Table 1 presents the skewness and kurtosis values, which reveal that  $TiO_2$ ,  $Fe_2O_3$ ,  $MnO$ ,  $K_2O$ ,  $CaO$ , Cr, Cu, Zn, and Ba exhibited values higher than zero, whereas the remaining elements displayed skewness or kurtosis values lower than zero. Table 1 also documents the geochemical threshold values used to separate anomalies from background values for the 26 elements in river sands from the study area. These threshold values were determined using the mean+2STD, median+2MAD, and TIF methods. Anomaly threshold values obtained from statistical approaches that exceeded the maximum measured values were excluded. Nb had a threshold value determined by the median+2MAD approach, whereas  $SiO_2$ ,  $Al_2O_3$ ,  $Na_2O$ , Co, Ga, Sr, Y, Zr, Nb, and Th had threshold values obtained from the mean+2STD method, which were greater than the maximum measured values. In addition,  $TiO_2$ ,  $CaO$ , Cr, Cu, Zn, and Ba exhibit threshold values lower than the maximum values derived from the TIF approach.

**Table 1.** Descriptive statistics for raw geochemical elements in river sands from the study area. All major element concentrations are given in weight percent (wt.%), and minor element contents are measured in parts per million (ppm)

Elements	Min.	Q25	Median	Q75	Max.	Mean	Mode	Std.	Variance	Range	Skew	Kurt	MAD	IQR	Mean+2Std	M+2MAD	TIF
<i>SiO<sub>2</sub></i>	36.84	49.25	52.47	54.60	59.94	51.55	54.53	4.82	23.212	23.10	-1.14	1.77	2.54	5.35	-	57.55	-
<i>TiO<sub>2</sub></i>	0.67	1.06	1.20	1.37	2.17	1.21	1.48	0.27	0.070	1.50	0.70	2.14	0.15	0.32	1.74	1.49	1.84
<i>Al<sub>2</sub>O<sub>3</sub></i>	9.97	13.20	14.10	16.20	17.90	14.50	13.20	1.93	3.739	7.93	-0.11	-0.56	1.30	3.00	-	16.70	-
<i>Fe<sub>2</sub>O<sub>3</sub></i>	4.75	7.20	8.19	9.24	11.94	8.18	-	1.54	2.369	7.19	0.33	0.16	1.03	2.04	11.26	10.24	-
<i>MnO</i>	0.09	0.17	0.18	0.23	0.32	0.19	0.16	0.04	0.002	0.23	0.43	0.25	0.02	0.07	0.28	0.23	-
<i>MgO</i>	1.66	2.65	3.12	3.76	4.70	3.20	2.98	0.75	0.559	3.04	0.08	-0.62	0.49	1.11	4.70	4.10	-
<i>Na<sub>2</sub>O</i>	1.06	1.81	2.11	2.47	2.79	2.09	2.06	0.43	0.181	1.73	-0.41	-0.28	0.34	0.66	-	2.79	-
<i>K<sub>2</sub>O</i>	0.68	1.28	1.40	1.63	2.15	1.45	-	0.29	0.084	1.47	0.35	0.61	0.14	0.35	2.03	1.68	-
<i>P<sub>2</sub>O<sub>5</sub></i>	0.15	0.18	0.20	0.22	0.27	0.20	0.21	0.03	0.001	0.12	-0.03	-0.31	0.02	0.04	0.26	0.24	-
<i>CaO</i>	4.93	6.86	10.00	12.54	24.25	10.50	-	4.49	20.185	19.32	1.39	2.23	3.02	5.68	19.49	16.03	21.05
<b>Cr</b>	49.00	126.50	166.00	205.50	1148.00	195.04	165.00	152.74	23328.152	1099.00	4.90	29.75	39.00	79.00	500.51	244.00	324.00
<b>Co</b>	0.00	36.00	59.00	79.00	109.00	56.36	0.00	28.69	823.310	109.00	-0.12	-0.80	21.00	43.00	-	101.00	-
<b>Ni</b>	23.00	45.50	56.00	70.50	103.00	58.93	46.00	17.63	310.840	80.00	0.42	-0.19	11.00	25.00	94.19	78.00	-
<b>Cu</b>	0.00	24.50	38.00	54.00	599.00	51.49	26.00	80.05	6408.140	599.00	6.38	44.08	14.00	29.50	211.59	66.00	98.25
<b>Zn</b>	38.00	81.00	97.00	109.00	240.00	95.72	81.00	30.07	904.250	202.00	1.95	9.31	16.00	28.00	155.86	129.00	151.00
<b>Ga</b>	0.00	13.00	21.00	30.50	41.00	21.08	0.00	11.36	129.150	41.00	-0.27	-0.86	9.00	17.50	-	39.00	-
<b>Rb</b>	0.00	42.50	62.00	74.50	115.00	58.60	61.00	25.71	661.130	115.00	-0.43	0.17	14.00	32.00	110.02	90.00	-
<b>Sr</b>	225.00	277.50	321.00	348.00	443.00	316.76	258.00	49.49	2449.150	218.00	0.36	-0.15	37.00	70.50	-	395.00	-
<b>Y</b>	0.00	15.50	26.00	38.50	52.00	25.42	0.00	14.70	216.020	52.00	-0.27	-0.88	12.00	23.00	-	50.00	-
<b>Zr</b>	65.00	162.00	196.00	209.50	265.00	184.51	167.00	40.27	1621.520	200.00	-0.73	0.63	22.00	47.50	-	240.00	-
<b>Nb</b>	0.00	4.50	18.00	28.50	38.00	16.81	0.00	12.51	156.390	38.00	0.004	-1.37	11.00	24.00	-	-	-
<b>Ba</b>	0.00	330.50	408.00	553.50	1718.00	483.26	396.00	303.92	92369.850	1718.00	1.950	5.33	104.00	223.00	1091.10	616.00	888.00
<b>Pb</b>	0.00	32.50	61.00	84.50	149.00	57.13	0.00	36.82	1356.000	149.00	0.08	-0.48	26.00	52.00	130.77	113.00	-
<b>Th</b>	0.00	0.00	22.00	48.50	73.00	26.17	0.00	24.61	605.680	73.00	0.41	-1.30	22.00	48.50	-	66.00	-
<b>Sc</b>	16.00	23.50	26.00	29.50	36.00	26.21	25.00	4.01	16.090	20.00	0.05	-0.09	3.00	6.00	34.23	32.00	-
<b>La</b>	0.00	18.00	38.00	53.00	85.00	36.17	0.00	23.06	531.680	85.00	0.08	-0.79	16.00	35.00	82.29	70.00	-

\* Min. = minimum; Max.= maximum; Q25 = first quartile (Q1); Q75 = third quartile (Q3); Std. = standard deviation; Skew = skewness; Kurt = kurtosis; MAD = median absolute deviations; IQR = interquartile range; mean+2STD = mean + 2 x standard deviations; M+2MAD = median + 2 x median absolute deviations; and TIF = Tukey's inner fence

To complement the descriptive statistics, distribution plots for the raw geochemical data of the river sands were generated. The distribution plots for Cr, Cu, Zn, and Ba are presented in Figure 3 and those for the remaining elements are provided in the Supplementary Material (Appendix A, Figures A1 and A2). The distribution plots for the analyzed geochemical elements primarily exhibited a normal distribution; however, those for Cr, Cu, Zn, and Ba deviated from the normal distribution.

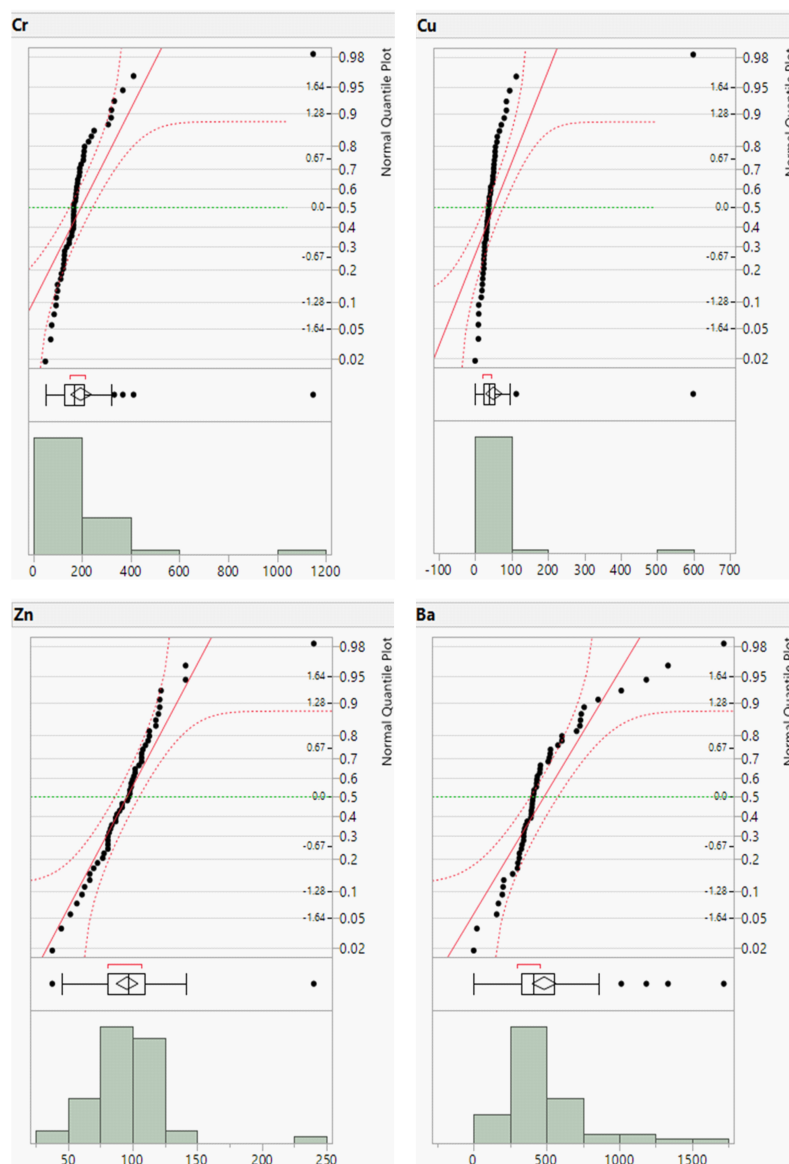


**Figure 3.** Distribution plots of Cr, Cu, Zn, and Ba concentrations (in ppm).

#### 4.2. Correlation and Multi-Element Relationships

The Spearman correlation coefficients between any pair of variables (elements) for the sampled river sands are presented in Table 2. The PCA results for the variables and samples are presented in Tables 3 and 4 as well as in Figures 4 and 5 (A and B). The percentages of variance explained by the first, second, third, and fourth principal components were 56.04%, 13.10%, 7.72% and 5.63%, respectively. According to the variable and sample results of the PCA as well as the component pattern biplot of the first and second principal components (PC1 and PC2), PC1 was strongly positively associated with Ga, Co, Y, La, Pb, Th,  $Al_2O_3$ , Nb, Zr, Ni, Rb,  $MgO$ ,  $Fe_2O_3$ ,  $Na_2O$ ,  $P_2O_5$ , Zn,  $SiO_2$ , Sc, Cr,  $TiO_2$ , and  $K_2O$ . The positive PC1 value had strong loadings for samples SS23, SS1, SS41, SS50, SS42, SS40, SS45, SS48, and others. Samples SS29, SS15, SS4, SS6, SS30, and others had a strong negative correlation with the

first principal component, and showed relative enrichment in  $CaO$  and  $Sr$ . The positive values of PC2 were strongly correlated with  $K_2O$ ,  $SiO_2$ ,  $Rb$ ,  $Ba$ , and  $Zn$ . These elements were highly concentrated in samples SS49, SS39, SS12, SS43, SS9, and SS13. PC2 had strong negative loadings for  $Sc$ ,  $MgO$ ,  $Fe_2O_3$ ,  $Cr$ , and  $TiO_2$ . These elements were abundant in samples SS4, SS45, SS11, SS29, and SS50. The component pattern biplot of the third and fourth principal components (PC3 and PC4) revealed that  $MnO$ ,  $Ba$ , and  $TiO_2$  had a strong positive association with PC3 and were enriched in samples SS15, SS49, SS13, and SS50. In contrast, the negative values of PC3 had a strong relationship with sample SS039 and were relatively abundant in  $Cu$  and  $Zn$ . In addition, samples SS039 and SS045 were strongly positively correlated with PC4 and were abundant in  $Cu$ ,  $Sr$ ,  $Zn$ , and  $MnO$ .

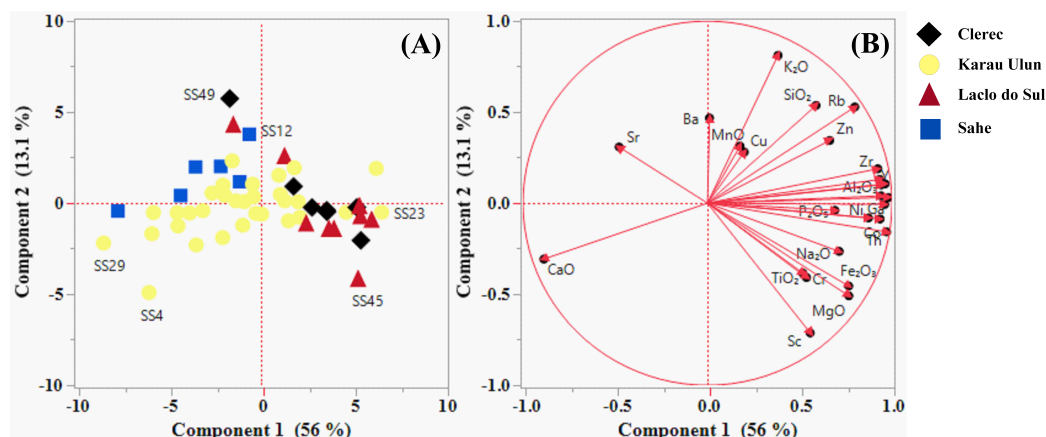


**Figure 4.** Samples (A) and variables (B) plotting on the first two component axes of the principal component analysis (PCA).

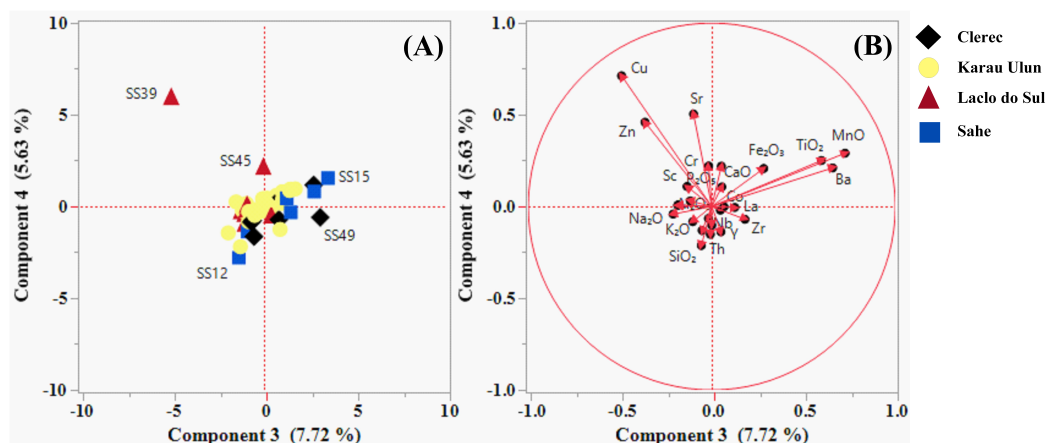


**Figure 5.** Samples (A) and variables (B) plotted on the third and fourth component axes of the PCA.

## 5. Discussion

### 5.1. Geochemistry and Provenance of River Sands

The concentration ranges of minor elements in Earth surface materials, as presented by Kabata-Pendias and Mukherjee [79], are provided in the Supplementary Material (Appendix A, Table A1) and can be used as references for the study area. Certain minor elements in basic rocks have higher concentrations than those in argillaceous rocks and sandstones, and vice versa. The basic and ultramafic rocks are identified by a significant percentage of mafic minerals [80], which typically contain higher concentrations of  $Cr$ ,  $Co$ ,  $Ni$ ,  $Cu$ , and  $Sc$  [79,81]. In the basic and ultramafic igneous rocks, the values of  $Cr$ ,  $Co$ ,  $Ni$ ,  $Cu$ ,  $Nb$ , and  $Sc$  range from 170-3400, 35-200, 130-160, 10-120, 10-35, and 5-35 ppm, respectively. In addition, argillaceous rocks are characterized by a significant proportion of clay

minerals [82]. However, carbonate materials are also abundant and have been found to be integrated into sediment and sedimentary rocks in different proportions [83]. The concentrations of Zn, Ga, Rb, Sr, Ba, Pb, Th, and La in the argillaceous sedimentary rocks range from 80-120, 15-25, 120-200, 300-450, 500-800, 14-40, 10-12, and 30-90 ppm, respectively. The values of Y and Zr in the sandstones vary from 15-250 and 180-250 ppm, respectively.

The high concentrations of Cr, Cu, and Zn recorded in the river sands in the study area can be attributed to the occurrence of chromite and Cu-Zn mineral deposits [84,85]. Ba, Sr, and Rb are widely recognized as mobile elements that are often depleted in river sands because of their mobility and leachability during weathering [86,87]. However, the high

The Spearman correlation coefficient results (Table 2) revealed that the contribution from the destruction of carbonate, clay, mica, and feldspar minerals was reflected in the negative correlation between most of the minor elements and Sr and  $CaO$ , significant positive associations between most minor elements and Ga and  $Al_2O_3$ , and significant positive correlations between  $K_2O$  and Rb and Pb and Rb. Ba displayed a positive relationship with  $K_2O$ , Rb, and Sr. Moderate-to-strong positive associations were observed among Cr, Co, Ni, Sc,  $TiO_2$ ,  $Fe_2O_3$ , and  $MgO$ , likely reflecting the contributions of minerals such as chromite, garnet, olivine, pyroxene, amphibole, sphene, rutile, hematite, ilmenite, magnetite, biotite, and chlorite to the river sand compositions.

The major contributions of clastic sedimentary rocks (such as shales, claystones, siltstones, and mudstones), mafic igneous rocks with chromite deposits, carbonate sedimentary rocks, metamorphic rocks, and Cu-Zn deposits in the river sands were confirmed by observing the distribution plots of minor elements (Figure 3 and Supplementary Materials in Appendix A, Figures A1 and A2), comparing the concentrations of minor elements with the range in concentrations presented by Kabata-Pendias and Mukherjee [79], and the results of the Spearman correlation coefficient [81,84,89–91]. The potential occurrence of hydrothermal and metamorphic processes, along with the presence of clastic and carbonate sedimentary, igneous, and metamorphic rocks in the study area, has been reported by Vilanova et al. [78].

The PCA results showed that the pattern plot of PC1 and PC2 (Tables 3 and 4; Figure 4) defined the geochemical associations of elements related to the origin and composition of the underlying lithologies, whereas PC3 and PC4 (Tables 3 and 4; Figure 5) allowed identification of the presence and distribution of deposits and alteration minerals associated with the effects of metamorphism and hydrothermal processes in the study area. The PCA findings corroborate the aforementioned results.

**Table 2.** Non-parametric correlation coefficient (Spearman) between geochemical elements in the river sands from the study area. The correlations between elements discussed in the text are denoted by boldface type

	SiO <sub>2</sub>	TiO <sub>2</sub>	Al <sub>2</sub> O <sub>3</sub>	Fe <sub>2</sub> O <sub>3</sub>	MnO	MgO	Na <sub>2</sub> O	K <sub>2</sub> O	P <sub>2</sub> O <sub>5</sub>	CaO	Cr	Co	Ni	Cu	Zn	Ga	Rb	Sr	Y	Zr	Nb	Ba	Pb	Th	Sc	La	
SiO <sub>2</sub>	—																										
TiO <sub>2</sub>	-0.03	—																									
Al <sub>2</sub> O <sub>3</sub>	0.52	0.39	—																								
Fe <sub>2</sub> O <sub>3</sub>	0.02	0.76	0.66	—																							
MnO	0.23	0.50	0.08	0.20	—																						
MgO	0.18	0.45	0.79	0.78	-0.01	—																					
Na <sub>2</sub> O	0.49	0.44	0.77	0.61	0.17	0.74	—																				
K <sub>2</sub> O	0.45	-0.13	0.41	-0.03	0.11	-0.01	0.02	—																			
P <sub>2</sub> O <sub>5</sub>	0.06	0.47	0.59	0.68	0.17	0.55	0.50	0.37	—																		
CaO	-0.76	-0.30	-0.90	-0.53	-0.21	-0.65	-0.72	-0.51	-0.49	—																	
Cr	0.24	<b>0.51</b>	<b>0.76</b>	<b>0.81</b>	0.13	<b>0.88</b>	0.68	0.01	0.53	<b>-0.68</b>	—																
Co	0.37	<b>0.60</b>	<b>0.87</b>	<b>0.87</b>	0.18	<b>0.84</b>	0.72	0.24	0.68	<b>-0.82</b>	<b>0.90</b>	—															
Ni	0.29	<b>0.34</b>	<b>0.84</b>	<b>0.69</b>	0.06	<b>0.86</b>	0.62	0.31	0.61	<b>-0.77</b>	<b>0.89</b>	<b>0.87</b>	—														
Cu	0.29	0.47	<b>0.81</b>	0.75	0.22	0.70	0.62	0.35	0.75	<b>-0.73</b>	0.74	0.85	0.79	—													
Zn	0.48	0.35	<b>0.88</b>	0.62	0.12	0.67	0.57	0.53	0.58	<b>-0.86</b>	0.69	0.84	0.79	0.89	—												
Ga	0.49	0.49	<b>0.92</b>	0.79	0.16	0.78	<b>0.71</b>	0.37	<b>0.65</b>	<b>-0.90</b>	0.84	0.97	0.86	0.84	0.89	—											
Rb	0.58	0.13	<b>0.76</b>	0.37	0.15	0.41	0.38	<b>0.80</b>	0.45	<b>-0.84</b>	0.46	0.67	0.66	0.64	0.83	0.77	—										
Sr	-0.27	-0.30	<b>-0.40</b>	-0.49	0.06	-0.52	-0.34	0.01	-0.22	<b>0.48</b>	<b>-0.40</b>	<b>-0.53</b>	<b>-0.36</b>	<b>-0.34</b>	<b>-0.40</b>	<b>-0.51</b>	-0.33	—									
Y	0.59	0.48	<b>0.91</b>	0.70	0.19	0.72	0.70	0.42	0.56	<b>-0.94</b>	0.78	0.93	0.81	0.76	0.87	0.97	0.81	<b>-0.53</b>	—								
Zr	0.53	0.50	<b>0.81</b>	0.69	0.24	0.62	0.56	0.47	0.56	<b>-0.87</b>	0.70	0.88	0.74	0.72	0.83	0.92	0.82	<b>-0.56</b>	0.94	—							
Nb	0.63	0.38	<b>0.87</b>	0.64	0.20	0.69	0.65	0.49	0.54	<b>-0.96</b>	0.74	0.90	0.80	0.78	0.89	0.95	0.84	<b>-0.54</b>	0.97	0.92	—						
Ba	0.06	0.45	0.12	0.25	0.42	-0.05	-0.07	<b>0.29</b>	0.21	<b>-0.18</b>	0.15	0.22	0.13	0.23	0.27	0.24	<b>0.28</b>	<b>0.22</b>	0.27	0.37	0.25	—					
Pb	0.39	0.45	<b>0.87</b>	0.77	0.19	0.70	0.61	0.46	0.70	<b>-0.84</b>	0.80	0.93	0.83	0.84	0.86	0.95	0.82	<b>-0.40</b>	0.91	0.89	0.91	0.30	—				
Th	0.51	0.48	<b>0.89</b>	0.76	0.21	0.73	0.67	0.39	0.60	<b>-0.91</b>	0.79	0.94	0.81	0.82	0.88	0.97	0.79	<b>-0.52</b>	0.96	0.92	0.96	0.26	0.94	—			
Sc	0.01	<b>0.50</b>	0.56	<b>0.73</b>	-0.13	<b>0.76</b>	0.60	-0.24	0.41	<b>-0.40</b>	<b>0.68</b>	<b>0.66</b>	<b>0.55</b>	0.51	0.47	0.58	0.15	<b>-0.49</b>	0.52	0.47	0.45	-0.09	0.48	0.55	—		
La	0.44	0.60	<b>0.87</b>	0.82	0.23	0.76	0.67	0.37	0.65	<b>-0.86</b>	0.81	0.96	0.83	0.83	0.87	0.97	0.75	<b>-0.50</b>	0.95	0.91	0.93	0.30	0.94	0.95	0.56	—	

**Table 3.** Variable results of the PCA for the first four components with eigenvalues greater than 1.0. Loading values are presented for variables with values greater than +0.3 and less than -0.3.

	PC1	PC2	PC3	PC4		PC1	PC2	PC3	PC4
<b>Eigenvalues</b>	<b>14.57</b>	<b>3.41</b>	<b>2.01</b>	<b>1.46</b>	<b>Eigenvalues</b>	<b>14.57</b>	<b>3.41</b>	<b>2.01</b>	<b>1.46</b>
<b>Explanation (%)</b>	<b>56.04</b>	<b>13.1</b>	<b>7.72</b>	<b>5.63</b>	<b>Explanation (%)</b>	<b>56.04</b>	<b>13.1</b>	<b>7.72</b>	<b>5.63</b>
<i>SiO<sub>2</sub></i>	0.582	0.519			<b>Cu</b>			-0.496	0.737
<i>TiO<sub>2</sub></i>	0.504	-0.374	0.675		<b>Zn</b>	0.635	0.338	-0.396	0.484
<i>Al<sub>2</sub>O<sub>3</sub></i>	0.939				<b>Ga</b>	0.983			
<i>Fe<sub>2</sub>O<sub>3</sub></i>	0.773	-0.479			<b>Rb</b>	0.790	0.502		
<i>MnO</i>			0.745	0.307	<b>Sr</b>	-0.504			0.509
<i>MgO</i>	0.776	-0.506			<b>Y</b>	0.965			
<i>Na<sub>2</sub>O</i>	0.718				<b>Zr</b>	0.923			
<i>K<sub>2</sub>O</i>	0.364	0.816			<b>Nb</b>	0.936			
<i>P<sub>2</sub>O<sub>5</sub></i>	0.685				<b>Ba</b>		0.469	0.705	
<i>CaO</i>	-0.882				<b>Pb</b>	0.941			
<b>Cr</b>	0.519	-0.394			<b>Th</b>	0.940			
<b>Co</b>	0.975				<b>Sc</b>	0.569	-0.743		
<b>Ni</b>	0.872				<b>La</b>	0.962			

**Table 4.** Sample results for the first four components of the PCA. Loading values for samples with values greater than +2.0 and less than -2.0 are shown in bold.

	PC1	PC2	PC3	PC4		PC1	PC2	PC3	PC4
<b>Eigenvalues</b>	<b>14.57</b>	<b>3.41</b>	<b>2.01</b>	<b>1.46</b>	<b>Eigenvalues</b>	<b>14.57</b>	<b>3.41</b>	<b>2.01</b>	<b>1.46</b>
<b>Explanation (%)</b>	<b>56.04</b>	<b>13.1</b>	<b>7.72</b>	<b>5.63</b>	<b>Explanation (%)</b>	<b>56.04</b>	<b>13.1</b>	<b>7.72</b>	<b>5.63</b>
<b>SS1</b>	<b>6.241</b>	1.910	-0.167	-0.279	<b>SS28</b>	-1.369	0.128	-0.044	0.422
<b>SS2</b>	1.795	1.945	-0.840	-0.266	<b>SS29</b>	<b>-8.541</b>	<b>-2.186</b>	-1.950	-1.434
<b>SS3</b>	<b>-2.082</b>	-1.894	-0.521	-0.407	<b>SS30</b>	<b>-5.838</b>	-0.517	-1.524	0.255
<b>SS4</b>	<b>-6.080</b>	<b>-4.906</b>	-0.515	-0.484	<b>SS31</b>	<b>-3.878</b>	-0.540	-0.939	-0.138
<b>SS5</b>	-0.410	0.349	1.025	0.455	<b>SS32</b>	<b>-2.069</b>	0.997	-1.185	-0.219
<b>SS6</b>	<b>-5.920</b>	-1.675	-0.853	-0.827	<b>SS33</b>	<b>-4.552</b>	-0.524	0.144	-0.006
<b>SS7</b>	1.277	0.131	0.166	0.454	<b>SS34</b>	-1.158	1.178	1.457	-0.317
<b>SS8</b>	1.041	0.483	0.148	-0.189	<b>SS35</b>	<b>2.759</b>	-0.232	0.805	-0.712
<b>SS9</b>	-1.570	<b>2.325</b>	0.873	-1.247	<b>SS36</b>	-1.977	0.428	0.453	0.364
<b>SS10</b>	<b>2.101</b>	-0.774	-1.291	-2.191	<b>SS37</b>	-0.290	-0.559	0.990	0.809
<b>SS11</b>	<b>-3.520</b>	<b>-2.292</b>	-0.501	-0.170	<b>SS38</b>	<b>-2.657</b>	0.558	-0.406	-0.260
<b>SS12</b>	-0.632	<b>3.786</b>	-1.375	-2.795	<b>SS39</b>	-1.509	<b>4.305</b>	<b>-5.062</b>	<b>5.982</b>
<b>SS13</b>	<b>-2.188</b>	<b>2.016</b>	<b>2.731</b>	0.817	<b>SS40</b>	<b>5.329</b>	-0.149	-1.263	-0.236
<b>SS14</b>	<b>-3.546</b>	1.994	-0.891	-1.376	<b>SS41</b>	<b>5.991</b>	-0.907	-0.933	0.090
<b>SS15</b>	<b>-7.762</b>	-0.435	<b>3.481</b>	1.546	<b>SS42</b>	<b>5.387</b>	-0.705	-1.064	-0.381
<b>SS16</b>	<b>-4.358</b>	0.418	1.244	0.451	<b>SS43</b>	1.270	<b>2.588</b>	0.389	-0.473
<b>SS17</b>	0.961	1.531	-1.053	-0.293	<b>SS44</b>	<b>3.672</b>	-1.408	-0.843	-0.078
<b>SS18</b>	-0.465	1.047	-0.961	0.166	<b>SS45</b>	<b>5.258</b>	<b>-4.152</b>	-0.039	<b>2.173</b>
<b>SS19</b>	1.482	-0.967	1.393	0.872	<b>SS46</b>	<b>3.949</b>	-1.411	-0.963	-0.155
<b>SS20</b>	<b>2.010</b>	0.079	1.010	0.310	<b>SS47</b>	<b>2.445</b>	-1.105	-1.047	-0.922
<b>SS21</b>	0.032	-0.602	1.697	0.960	<b>SS48</b>	<b>5.193</b>	-0.235	0.951	0.499
<b>SS22</b>	<b>4.610</b>	-0.499	0.333	-0.288	<b>SS49</b>	-1.696	<b>5.748</b>	<b>3.063</b>	-0.590
<b>SS23</b>	<b>6.534</b>	-0.502	0.938	0.173	<b>SS50</b>	<b>5.409</b>	<b>-2.045</b>	<b>2.706</b>	1.177
<b>SS24</b>	<b>-4.508</b>	-1.248	-0.083	0.422	<b>SS51</b>	<b>3.578</b>	-0.471	-0.622	-0.750
<b>SS25</b>	-0.995	-1.209	1.446	0.951	<b>SS52</b>	<b>3.554</b>	-0.393	-0.681	-0.851
<b>SS26</b>	<b>-3.164</b>	-0.407	0.059	0.023	<b>SS53</b>	1.763	0.918	-0.551	-1.636
<b>SS27</b>	-0.905	0.088	0.665	0.603					

concentrations of Sr and Ba measured in the study area are likely due to specific source compositions or materials of the original rocks and specific geological processes, such as hydrothermal alterations [85,88].

The pattern plot of PC1 may effectively separate the presence and distribution of compositional variations between the carbonate- and non-carbonate-rich river sands from the study area. Carbonate minerals, such as calcite and aragonite, which are commonly affiliated with carbonate sedimentary rocks, may have significantly contributed to the elemental association observed in the negative scores of PC1. This component was prominently recorded at sample locations SS29, SS15, SS4, SS6, and

SS30, which were mainly drained from the Aitutu, Viqueque, and Wailuli Formations. The elemental relationship seen in the positive values of PC1 may have been strongly influenced by non-carbonate minerals, such as clay, mica, quartz, feldspar, heavy, and other accessory minerals, which are frequently associated with clastic sedimentary rocks. The elemental association observed in these positive values was highly concentrated in sample locations SS23, SS1, SS41, SS50, SS42, SS40, SS45, and SS48, which were primarily drained from the Wailuli, Viqueque, and Aitutu Formations, as well as the Bobonaro Complex. The PC2 pattern plot effectively captures the compositional variations between the mafic and non-mafic-rich river sands within the study area. The contributions of chromite, garnet, spinel, olivine, pyroxene, amphibole, biotite, magnetite, sphene, ilmenite, and chlorite affiliated with igneous, metamorphic, and clastic sedimentary rocks were responsible for the negative PC2 scores. Representing this component, samples SS4, SS45, SS11, SS29, and SS50 were collected from areas drained from the Lolotoi and Bobonaro Complexes as well as from the Ainaro, Viqueque, and Wailuli Formations. The igneous and metamorphic rocks associated with the Bobonaro Complex were identified as exotic blocks that were incorporated into clastic sedimentary rocks (such as shales and mudstones) [92]. The elemental association observed in the positive values of PC2 was potentially consistent with the relative abundance of feldspar, quartz, mica, and clay minerals in the river sands. These minerals can be attributed to the presence of clastic sedimentary rocks and their altered rocks owing to metamorphic processes. The elemental relationship observed in these positive scores was highly reported in samples SS49, SS39, SS12, SS43, SS9, and SS13, which were collected from areas drained from the Wailuli Formation and Dilor Conglomerate.

### 5.2. Influence of Mineral Deposit Potential on the Geochemical Characteristics of River Sands

The statistical parameters of the raw geochemical elements, particularly skewness and kurtosis, indicated that Cr, Cu, Zn, and Ba had values greater than 1 and 3, respectively. These elements also exhibited relatively noticeable differences in the mean, median, and mode values. For  $CaO$ , the skewness value was greater than 1, whereas the kurtosis value was less than 3. The threshold values for  $TiO_2$ ,  $CaO$ , Cr, Cu, Zn, and Ba were obtained using these three methods. The threshold values achieved by the methods followed the decreasing order  $TIF > mean+2STD > median+2MAD$  for  $TiO_2$  and  $CaO$ , whereas Cr, Cu, Zn, and Ba decreased in the order  $mean+2STD > TIF > median+2MAD$ . The TIF approach values corresponded closely to the upper inner fence values of the boxplot [65,66,93], and the results of this approach were used as the threshold values [67,68].

Five geochemical classes for the concentrations of Cr, Cu, Zn, and Ba were identified using the boxplot model [69], as shown in Table 5. A distribution map of geochemical classes for Cr, Cu, Zn, and Ba in the study area was delineated using the IDW method for gridding and illustrating the spatial distributions of geochemical anomalies (Figure 6). Anomalous values of Cr were observed in the midstream to downstream areas of the Laclo do Sul River basin. In contrast, anomalous values of Ba were concentrated in the northern branch of the Clerec River catchment, midstream areas of the Sahe River basin, and midstream areas of the western branch of the Karau Ulun River catchment. In addition, the nearly identical spatial distribution patterns of Cu and Zn likely indicated that they were derived from the same source materials [94]. Anomalous values of Cu and Zn were observed in the midstream area of the Laclo do Sul basin.

The positive PC3 and PC4 values as well as the negative PC2 and PC3 scores were subjected to distribution plots (Figure 7) to separate the five geochemical populations with extremely low background, low background, background, high background, and anomalies (Table 6). Five distinct geochemical classes were delineated using the IDW approach for gridding and illustrating the spatial distributions of anomalous values from the selected PCA components in the study area (Figure 8).

**Table 5.** Geochemical classes derived from the boxplot model for Cr, Cu, Zn, and Ba concentrations (in ppm) in river sands from the study area

Geochemical Class	Calculated Values (in ppm)			
	Cr	Cu	Zn	Ba
Extremely low background	-	-	38.00-45.00	-
Low background	49.00-126.50	0.00-24.50	45.00-81.00	0.00-330.50
Background	126.50-205.50	24.50-54.00	81.00-109.00	330.50-553.50
High background	205.50-324.00	54.00-98.25	109.00-151.00	553.50-888.00
Anomaly	324.00-1148.00	98.25-599.00	151.00-240.00	888.00-1718.00

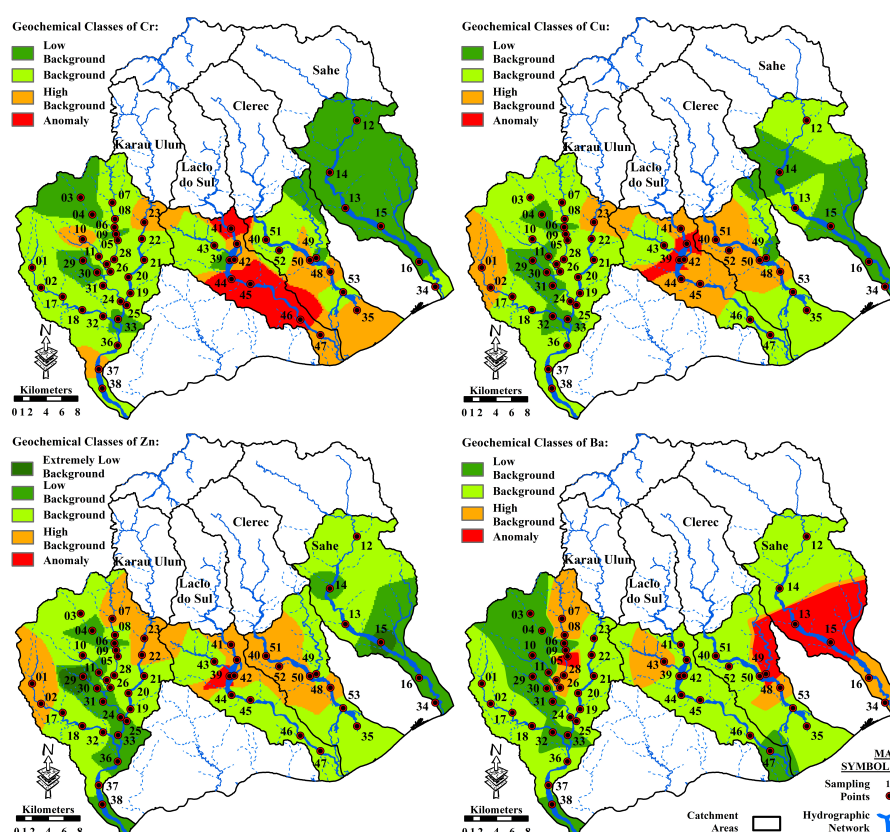


**Figure 6.** Distribution of geochemical classes for Cr, Cu, Zn, and Ba in the study area, derived from the boxplot model.

Sc, MgO, Fe<sub>2</sub>O<sub>3</sub>, Cr, and TiO<sub>2</sub> were grouped together on the negative side of PC2, likely reflecting the presence of mafic, heavy, and accessory minerals concentrated in the igneous and metamorphic rocks [84,91,95]. However, the high anomalous value distributions of Cr and elemental associations in the negative PC2 scores (Figures 6 and 8) may be related to the presence of igneous rocks (basic and ultramafic) containing chromite mineral deposits [78,85]. The samples representing these anomalies were collected from areas that were drained from the Lolotoi and Bobonaro Complexes, particularly in the upstream areas of the northwestern branch of the Karau Ulun River catchment and the midstream areas of the Laçlo do Sul basin. The existence of igneous rocks with chromite mineral deposits associated with the Bobonaro Complex as exotic blocks were incorporated into shales and mudstones [92].

**Table 6.** Geochemical classes derived from the boxplot models for the positive PC3 and PC4 scores and negative values of PC2 and PC3.

	Geochemical Class				
	Extremely low background	Low background	Background	High background	Anomaly
Negative score of PC2	-	-	0.00-(-0.94)	(-0.94)-(-2.29)	(-2.34)-(-4.91)
Positive score of PC3	-	-	0.00-0.94	0.94-1.70	2.36-3.48
Negative value of PC3	-	-	0.00-(-0.94)	(-0.94)-(-1.95)	(-2.34)-(-5.06)
Positive value of PC4	-	-	0.00-0.45	0.45-0.96	1.13-5.98

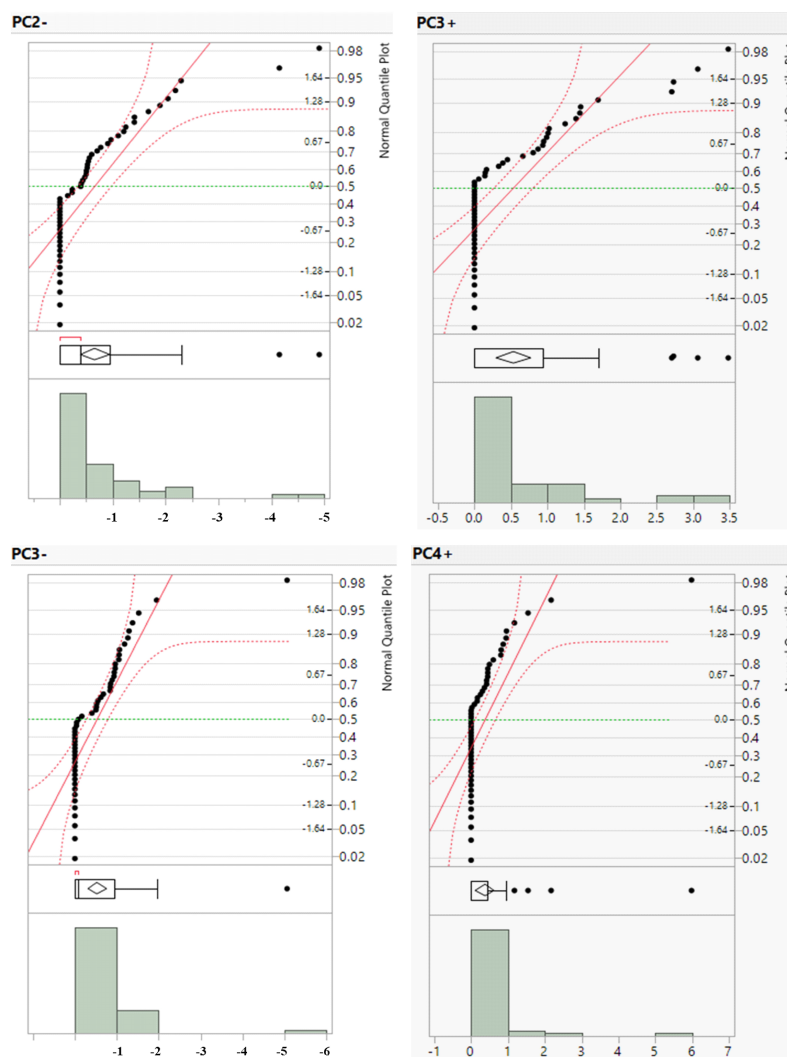


**Figure 7.** Distribution plots of the positive PC3 and PC4 scores, as well as the negative values of PC2 and PC3.

The occurrence of a potential mineralization zone dominated by Cu and Zn could explain their high anomalous value distributions, as well as the elemental relationships in the negative PC3 scores [84,90], in the midstream areas of the Lacro do Sul River basin (Figures 6 and 8). This anomaly was particularly evident in the sample drained from clastic sedimentary rocks and the altered rocks of the Wailuli Formation, which could be the host rocks for the Cu-Zn mineralization.

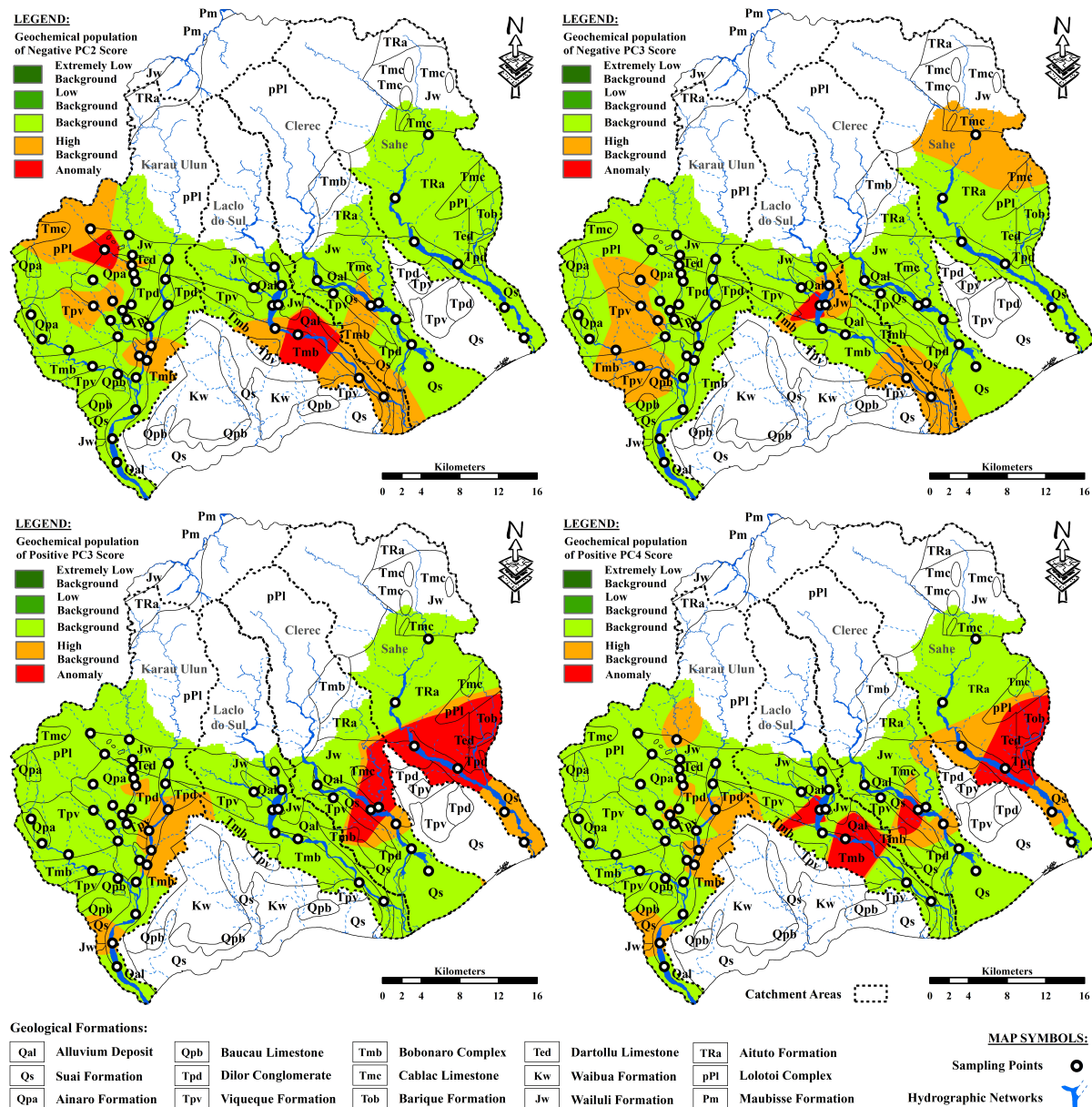


**Figure 8.** Distribution of geochemical anomalies for the elemental association of the negative PC2 and PC3, as well as the positive PC3 and PC4 values, derived from the boxplot model.

Overall, the contributions of carbonate, feldspar, mica, clay, amphibole, and biotite were most likely responsible for the presence and distribution of Ba [81,89] in the river sands of the study area. However, the high anomalous value distributions of Ba and the elemental association of  $MnO$ -Ba- $TiO_2$  in the positive PC3 scores likely indicate the occurrence of secondary alteration mineral assemblages, such as barite, manganese, rutile, and goethite [85,96]. The distribution of geochemical classes for positive PC3 values in the study area shows that anomalous values of this component were concentrated in the northern branch and downstream areas of the Clerec River catchment, as well as in the midstream areas of the Sahe River basin (Figure 8). Samples carrying these anomalies were collected from locations drained from carbonate sedimentary rocks and altered rocks because of metamorphic and hydrothermal processes in the Aitutu and Wailuli Formations.

The elemental association observed in the positive PC4 scores could be significantly influenced by the occurrence of the Cu-Zn deposits, as well as carbonate and manganese minerals [84,85,90], which are associated with carbonate and clastic sedimentary rocks and their altered rocks owing to

metamorphic and hydrothermal processes. Anomalous values of this component were observed in the midstream areas of the Lacro do Sul, Clerec, and Sahe River catchments (Figure 8). These anomalies were most noticeable in the sample drained from the Aitututu and Wailuli Formations, as well as the Bobonaro Complex. The presence of carbonate and clastic sedimentary rocks and their altered rocks are associated with the Bobonaro Complex as exotic blocks incorporated into shales and mudstones [92].

### 5.3. Prediction of Target Areas for Future Research and Exploration

Four potential target areas for mineral deposits were identified in the study area and proposed for further study and exploration, as illustrated in Figure 9. Target areas A and B show evident distributions of anomalous values of Cr and elemental assemblages with the negative PC2 scores, as shown in Figures 6 and 8. The distributions of anomalous values of Cu and Zn as well as the elemental association with negative PC3 scores (Figures 6 and 8), corresponded well with the delineation of target area C. In addition, the proposed boundary of target area D is consistent with the distribution of anomalous Ba values and anomalous scores of multi-element relationships in the positive PC3 and PC4.

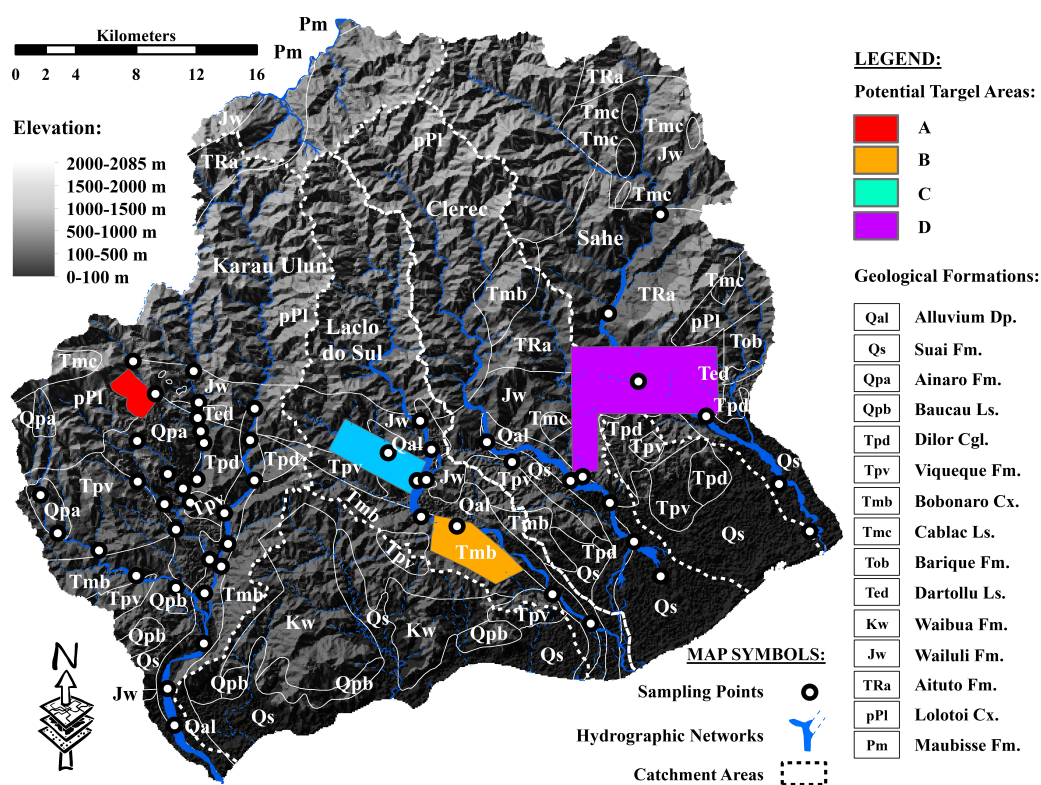


Figure 9. Proposed potential target areas for mineral deposits in the study area.

## 6. Conclusions

The characteristics of Cr, Cu, Zn, and Ba in the river sands of the study area fell outside a normal distribution. The threshold estimated for these elements using the mean+2STD approach failed to yield adequate values, whereas the median+2MAD method delivered low threshold values, leading to the detection of the greatest number of outliers. This study presents the findings that the TIF and PCA methods are highly applicable and effective for calculating appropriate geochemical thresholds to separate anomalies from background values and identify relevant elemental associations. These approaches have proven useful for delineating target areas for mineral deposits, resulting in reliable outcomes [67,68,97,98].

Mafic, heavy, accessory, and clay minerals associated with igneous, metamorphic, and clastic sedimentary rocks significantly contributed to the varying concentrations of Cr, Cu, and Zn in most river sands in the study area. In addition, the Ba content was attributed to the important contributions from the destruction of carbonate and aluminum-rich minerals associated with carbonate and clastic sedimentary rocks. Target areas predicted for further geochemical studies and mineral exploration campaigns were delineated based on the distribution of several potential mineral deposit areas and hydrothermal alteration zones identified in the study area. Area A is spatially covered by the igneous rocks of the Lolotoi Complex, which are suspected to be the source of the detected geochemical anomalies and may indicate the presence of Cr deposits. Area B was identified as the source of the chromite deposits associated with the igneous and metamorphic rocks and was spatially affiliated with the Bobonaro Complex. In addition, area C is expected to be composed of clastic sedimentary rocks and altered rocks associated with the Wailuli Formation, which are considered potential hosts for mineralization dominated by Cu and Zn. Furthermore, area D is spatially occupied by carbonate and clastic sedimentary rocks affiliated with the Aitutu and Wailuli Formations, which are considered the source of the detected Ba geochemical anomalies and demonstrate possible evidence that these rocks have been significantly altered by hydrothermal processes.

The occurrence of hydrothermal mineralization associated with the Gondwana Megasequence has been reported previously by Vicente et al. [85]. Further geochemical studies and mineral exploration campaigns should be conducted in areas covered by the Wailuli Formation, particularly within the proposed boundary of target area D, because of the limited number of samples collected and the fact that several discoveries did not show significant geochemical anomalies [99], as demonstrated in the case study presented here. In addition, future studies should give greater attention and consideration to the presence of chromite deposits associated with the igneous rocks and altered clastic sedimentary rocks due to hydrothermal processes of the Wailuli Formation, which are incorporated into clastic sedimentary rocks as exotic blocks within the Bobonaro Complex [92]. However, no large outcrops of these exotic blocks have been found in the basin.

**Author Contributions:** V.V.: conceptualization, methodology, validation, investigation, formal analysis, writing—original draft. T.O.: validation, supervision, visualization, writing—review and editing. S.K.: validation, supervision, visualization, writing—review and editing. K.Y.: formal analysis. E.M.: investigation, formal analysis. All authors have read and agreed to the published version of the paper.

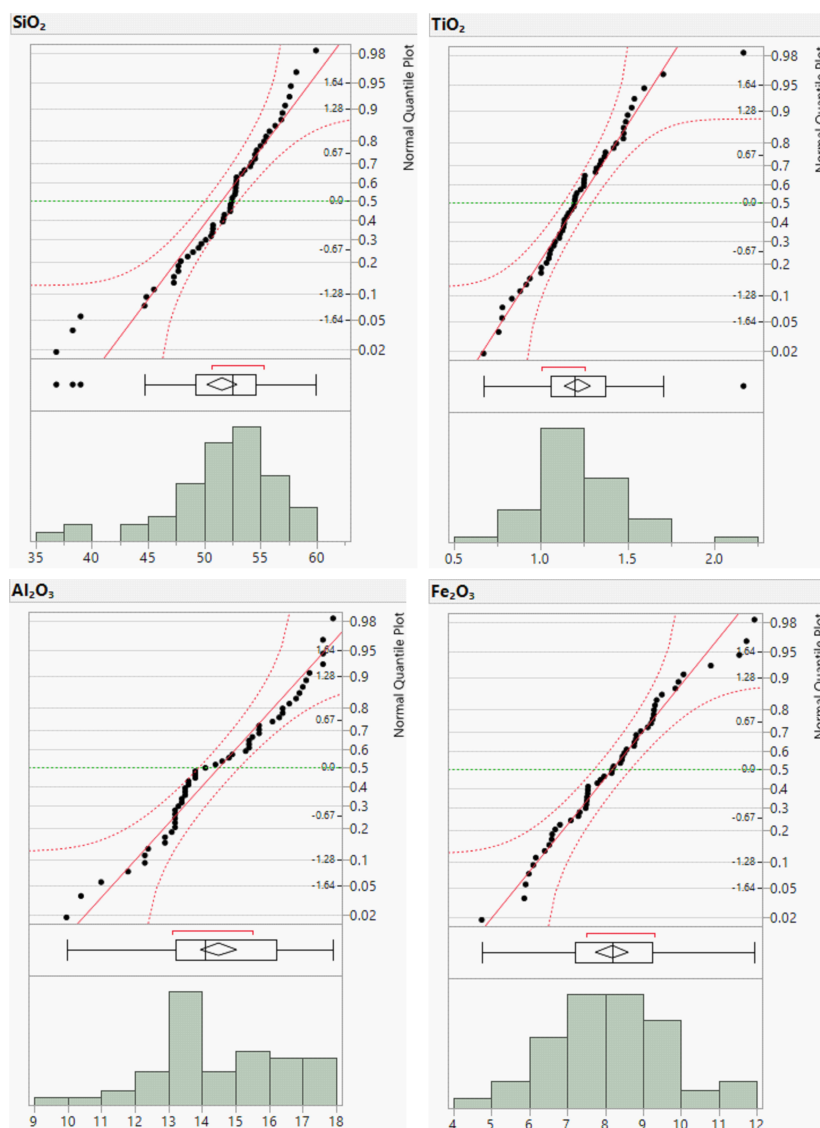
**Funding:** The Japan International Cooperation Agency (JICA) Development Studies Program, Human Resources Development in Science and Technology Innovation, and the Earth Science Laboratory, Faculty of Engineering, Gifu University provided funding for this study and covered the article processing charges (APC).

**Data Availability Statement:** All data included or referenced within this article are publicly available.

**Acknowledgments:** This study was made possible through the generous financial support of the Japan International Cooperation Agency (JICA) Development Studies Program and Human Resources Development in Science and Technology Innovation. We express our sincere appreciation to the staff of the Ministry of Petroleum and Mineral Resources, particularly Instituto de Geociências de Timor-Leste and the National Petroleum and Minerals Authority, Dili, Timor-Leste, for authorizing the shipment of samples from Timor-Leste to Japan. We also extend our gratitude to Professor Katsuta Nagayoshi and Mr. Matsuki of Gifu University for allowing us to take advantage of their laboratory facilities to prepare the glass bead samples. Finally, we would like to extend our heartfelt gratitude to the Nagoya University Museum, JICA and the dedicated staff members of the Faculty of Engineering at Gifu University, Prof. Dr. Koshi Yamamoto, Prof. Dr. Koichi Shimakawa, Mr. Atsushi Takahashi, Ms. Mieko Araki, Ms. Yukiko Eguchi, Ms. Naoko Yamada, and Ms. Midori Inuma.

**Conflicts of Interest:** The authors declare that there are no conflicts of interest, either financial or non-financial, that might affect the topic or findings of the research presented in this paper.

## Appendix A



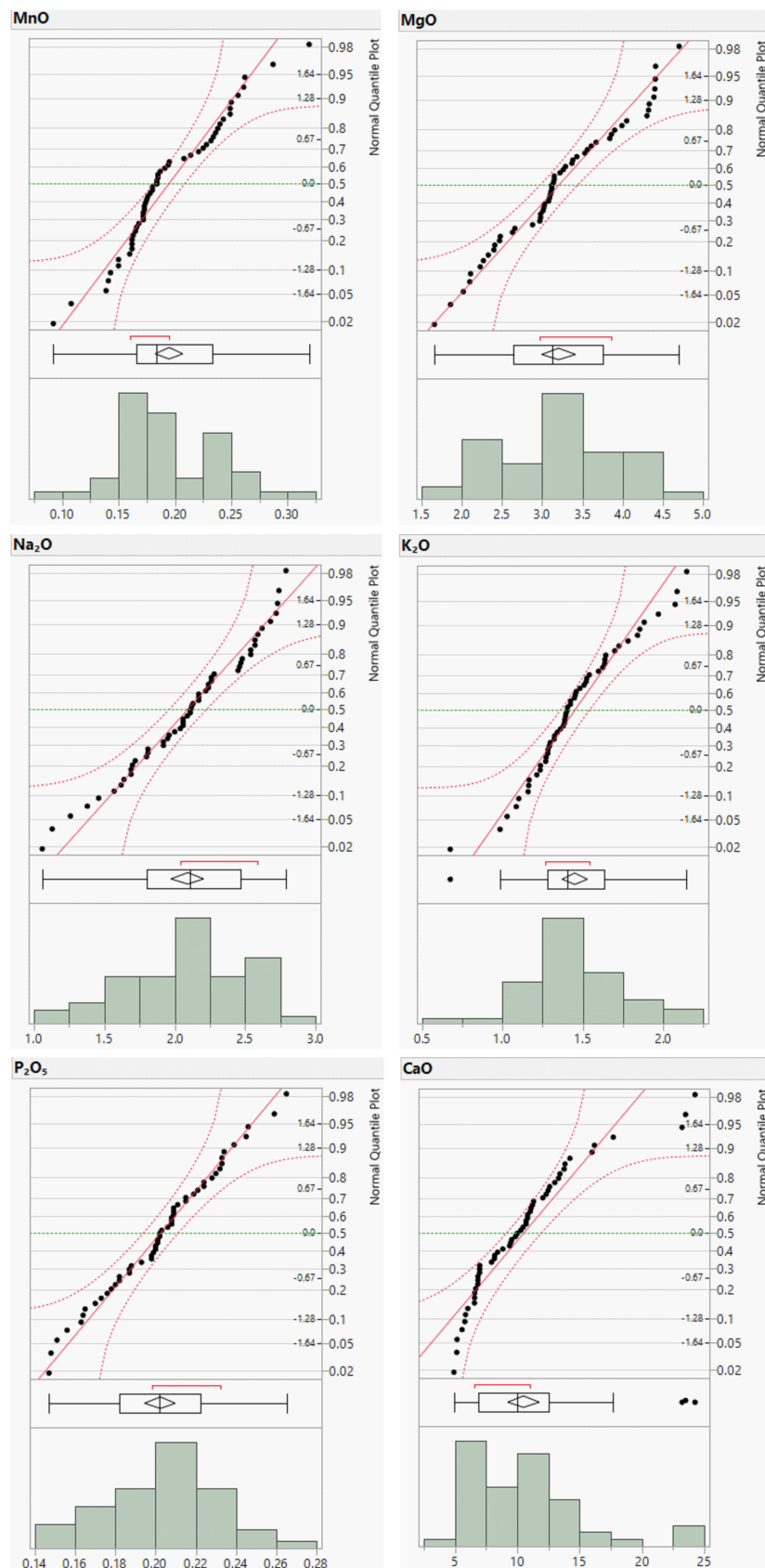
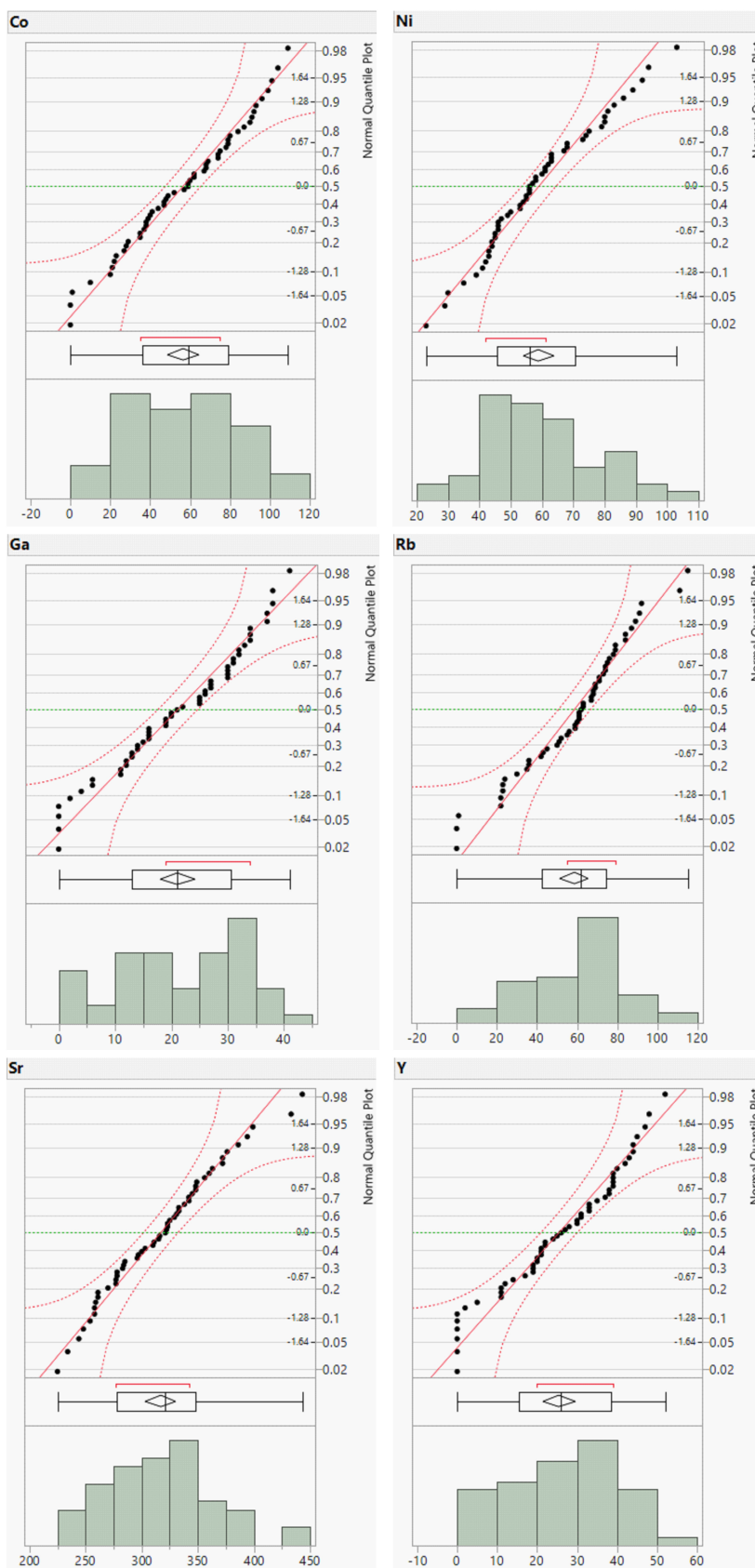


Figure A1. Distribution plots of major element concentrations (in wt.%).



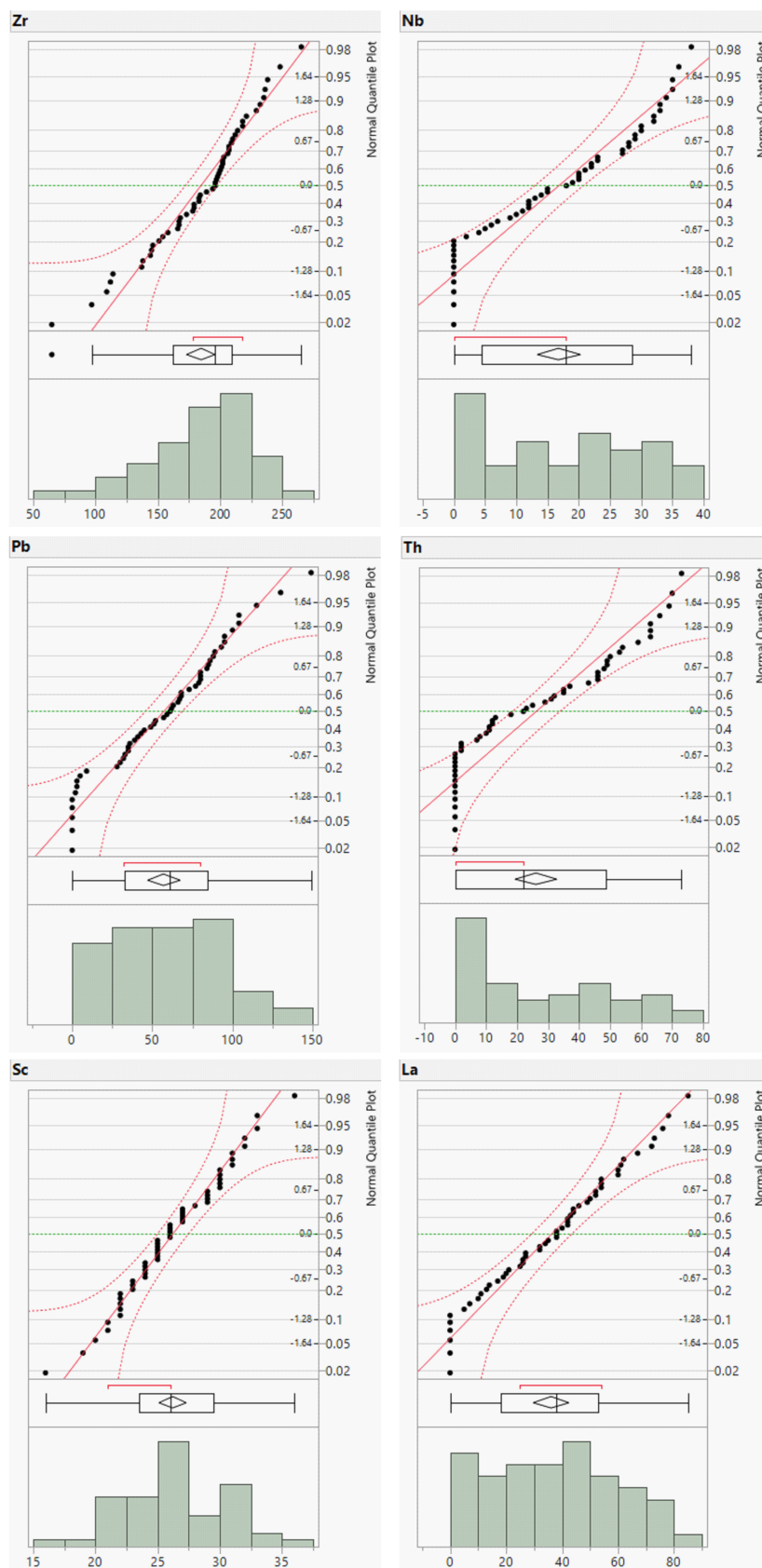


Figure A2. Distribution plots of minor element concentrations (in ppm).

**Table A1.** The abundance range values of minor elements in argillaceous, sandstone, and basic to ultramafic rocks (data from Kabata-Pendias and Mukherjee [79]).

Minor Elements	Basic-ultramafic igneous rocks (in ppm)	Argillaceous sedimentary rocks (in ppm)	Sandstones (in ppm)
Cr	170.0-3400.0	80.0-120.0	20.0-40.0
Co	35.0-200.0	14.0-20.0	0.3-10.0
Ni	130.0-160.0	40.0-90.0	5.0-20.0
Cu	10.0-120.0	40.0-60.0	5.0-30.0
Zn	40.0-120.0	80.0-120.0	15.0-30.0
Ga	15.0-24.0	15.0-25.0	5.0-12.0
Rb	2.0-45.0	120.0-200.0	10.0-45.0
Sr	140.0-460.0	300.0-450.0	20.0-140.0
Y	0.5-20.0	25.0-40.0	15.0-250.0
Zr	80.0-200.0	160.0-200.0	180.0-250.0
Nb	10.0-35.0	15.0-20.0	0.5-10.0
Ba	250.0-400.0	500.0-800.0	100.0-320.0
Pb	0.1-8.0	14.0-40.0	5.0-10.0
Th	1.0-14.0	10.0-12.0	2.0-4.0
Sc	5.0-35.0	10.0-15.0	1.0-3.0
La	2.0-70.0	30.0-90.0	17.0-40.0

## References

1. Franzinelli, E.; Potter, P. E. Petrology, Chemistry, and Texture of Modern River Sands, Amazon River System. *Journal of Geology*. **1983**, *91*, pp. 23–39.
2. He, J.; Garzanti, E.; Jiang, T.; Barbarano, M.; Resentini, A.; Liu, E.; Chen, S.; Shi, G.; Wang, H. Mineralogy and Geochemistry of Modern Red River Sediments (North Vietnam): Provenance and Weathering Implications. *Journal of Sedimentary Research*. **2022**, *92*, pp. 1169–1185. <https://doi.org/10.2110/jsr.2022.045>.
3. Liang, W.; Hu, X.; Garzanti, E.; Wen, H.; Hou, M. Petrographic Composition and Heavy Minerals in Modern River Sand: A Global Database. *Geoscience Data Journal*. **2023**, pp. 1–9. <https://doi.org/10.1002/gdj3.219>.
4. Tanaka, T.; Kawabe, i.; Hirahara, Y.; Iwamori, H.; Mimura, K.; Sugisaki, R.; Asahara, Y.; Ito, T.; Yurai, H.; Yonezawa, C.; Kanda, S.; Shimizu, O.; Hayasm, M.; Miura, N.; Mutoh, K.; Ohta, A.; Sugimura, K.; Togami, K.; Toriumi, T.; Matsumur, Y. Geochemical Survey of the Sanaga-Yama Area in Aichi Prefecture for Environmental Assessment. *J. Earth Planet. Sci. Nagoya Univ.*. **1994**, *41*, pp. 1–31.
5. Yamamoto, K.; Tanaka, T.; Minami, M.; Mimura, K.; Asahara, Y.; Yoshida, H.; Yogo, S.; Takeuchi, M.; Inayoshi, M. Geochemical Mapping in Aichi Prefecture, Japan: Its Significance as a Useful Dataset for Geological Mapping. *Applied Geochemistry*. **2007**, *22*, pp. 306–319. <https://doi.org/10.1016/j.apgeochem.2006.09.011>.
6. Dinis, P. A.; Sequeira, M.; Tavares, A. O.; Carvalho, J.; Castilho, A.; Pinto, M. C. Post-Wildfire Denudation Assessed from Compositional Features of River Sediments (Central Portugal). *Applied Clay Science*. **2020**, *193*, pp. 1–9. <https://doi.org/10.1016/j.clay.2020.105675>.
7. Vital, H.; Statterger, K. Major and Trace Elements of Stream Sediments from the Lowermost Amazon River. *Chemical Geology*. **2000**, *168*, pp. 151–168.
8. Nesbitt, H. W.; Young, G. M.; McLennan, S. M.; Keays, R. R. Effects of Chemical Weathering and Sorting on the Petrogenesis of Siliciclastic Sediments, with Implications for Provenance Studies. *Journal of Geology*. **1996**, *104*, pp. 525–542.
9. Grunsky, E. C.; Drew, L. J.; Sutphin, D. M. Process recognition in multi-element soil and stream-sediment geochemical data. *Applied Geochemistry*. **2009**, *24*, pp. 1602–1616. <https://doi.org/10.1016/j.apgeochem.2009.04.024>.
10. Johnsson, M. J. The System Controlling the Composition of Clastic Sediments. *Geological Society of America*. **1993**, *284*, pp. 1–21.
11. Cocker, M. D. Geochemical Mapping in Georgia, USA: A Tool for Environmental Studies, Geologic Mapping and Mineral Exploration. *Journal of Geochemical Exploration*. **1999**, *67*, pp. 345–360.
12. Oliva, P.; Viers, J.; Dupré, B. Chemical Weathering in Granitic Environments. *Chemical Geology*. **2003**, *202*, pp. 225–256.

13. Ottesen, R. T.; Theobald, P. K. Chapter 5: Stream Sediments in Mineral Exploration. In *Handbook of Exploration Geochemistry: Drainage Geochemistry*; Hale, M.; Plant, J. A., Eds.; Elsevier Science: Amsterdam, The Netherlands, **1994**; pp. 147–184.
14. Reimann, C.; Melezhik, V. Metallogenic Provinces, Geochemical Provinces and Regional Geology - What Causes Large-Scale Patterns in Low Density Geochemical Maps of the C-Horizon of Podzols in Arctic Europe?. *Applied Geochemistry*. **2001**, *16*, pp. 963–983.
15. Sawyer, E. W. The Influence of Source Rock Type, Chemical Weathering and Sorting on the Geochemistry of Clastic Sediments from the Quetico Metasedimentary Belt, Superior Province, Canada. *Chemical Geology*. **1986**, *55*, pp. 77–95.
16. Reimann, C.; Filzmoser, P. Normal and Lognormal data Distribution in Geochemistry: Death of a Myth. Consequence for the Statistical Treatment of Geochemical and Environmental Data. *Environmental Geology*. **1999**, *39*(9), pp. 1001–1014.
17. Reimann, C.; Ladenberger, A.; Birke, M.; De Caritat, P. Low Density Geochemical Mapping and Mineral Exploration: Application of the Mineral System Concept. *Geochemistry: Exploration, Environment, Analysis*. **2016**, *16*(1), pp. 48–61. <https://doi.org/10.1144/geochem2014-327>.
18. Carranza, E. J. M. Usefulness of Stream Order to Detect Stream Sediment Geochemical Anomalies. *Geochemistry: Exploration, Environment, Analysis*. **2004**, *4*(4), pp. 341–352. <https://doi.org/10.1144/1467-7873/03-040>.
19. Reimann, C.; Filzmoser, P.; Garrett, R. G. Background and Threshold: Critical Comparison of Methods of Determination. *Science of the Total Environment*. **2005**, *346*, pp. 1–16. <https://doi.org/10.1016/j.scitotenv.2004.11.023>.
20. Carranza, E. J. M. *Handbook of Exploration and Environmental Geochemistry: Geochemical Anomaly and Mineral Prospectivity Mapping in GIS*, 1st Ed., Vol. 11; Elsevier B.V.: The Netherlands, **2009**, 347 pp.
21. Davis, J. C. *Statistics and Data Analysis in Geology*, 3rd Ed.; John Willey & Sons: Kansas, U.S.A., **2002**, 257 pp.
22. Hawkes, H. E.; Webb, J. S. *SGeochemistry in Mineral Exploration*; Harper: New York, **1962**, 415 pp.
23. Reimann, C.; Filzmoser, P.; Garrett, R. G. Factor Analysis Applied to Regional Geochemical Data: Problems and Possibilities. *Applied Geochemistry*. **2002**, *17*, pp. 185–206.
24. Robinson, G. R.; Kapo, K. E.; Grossman, J. N. United State Geological Survey, New England, 2004. *Chemistry of Stream Sediments and Surface Waters in New England*, 18 pp.
25. Sinclair, A. J. Chapter 3: Univariate Analysis. In *Handbook of Exploration Geochemistry: Statistics and Data Analysis in Geochemical Prospecting*, Vol. 2; Howarth, R. J., Eds.; Elsevier Scientific Publishing Company, London, U. K., **1983**; pp. 59–83.
26. Tukey, J. W. *Exploratory Data Analysis*, Addison-Wesley Publishing Company: New Jersey, U.S.A., **1977**, 711 pp.
27. Zuo, R. Identifying Geochemical Anomalies Associated with Cu and Pb-Zn Skarn Mineralization Using Principal Component Analysis and Spectrum-Area Fractal Modeling in the Gangdese Belt, Tibet (China). *Journal of Geochemical Exploration*. **2011**, *111*, pp. 13–22. <https://doi.org/10.1016/j.gexplo.2011.06.012>.
28. Wittouck, S. F. Report of Allied Mining Corporation to Asia Investment. Co.Ltd., Kolff & Co., Batavia and Amsterdam, **1937**. *Exploration of Portuguese Timor*, 104 pp.
29. Leme, J. C. A. Junta de Investigações do Ultramar, Geólogo da Missão de Estudos Agronómicos do Ultramar, Lisboa, Portugal, **1968**. *Breve Ensaio Sobre a Geologia da Província de Timor*, Vol. I, pp 106–161.
30. Lacerda, V. P. A. Report for the Voluntary Mining and Energy Source Commission, Dili, East Timor, **1999**. *Data Statistik Bahan Galian Tambang Daerah Timor-Timur*, 50 pp.
31. ESCAP. Economic, and Social Commission for Asia and the Pacific, United Nations, New York, U.S.A., **2003**. *Atlas of Mineral Resources of the ESCAP Region: Geology and Mineral Resources of Timor-Leste.*, 177 pp.
32. Audley-Charles, M. G. Rates of Neogene and Quaternary Tectonic Movements in the Southern Banda Arc Based on Micropalaeontology. *Journal of the Geological Society, London*. **1986**, *143*, pp. 161–175.
33. Audley-Charles, M. G. Ocean Trench Blocked and Obliterated by Banda Forearc Collision with Australian Proximal Continental Slope. *Tectonophysics*. **2004**, *389*, pp. 65–79. <https://doi.org/10.1016/j.tecto.2004.07.048>.
34. Audley-Charles, M. G. Tectonic Post-Collision Processes in Timor. *The Geological Society of London, Special Publication*. **2011**, *355*, pp. 241–266. <https://doi.org/10.1144/SP355.12>.
35. Ely, K. S.; Sandiford, M.; Hawke, M. L.; Phillips, D.; Quigley, M.; Reis, J. E. dos. Evolution of Ataúro Island: Temporal constraints on subduction processes beneath the Wetar zone, Banda Arc. *Journal of Asian Earth Sciences*. **2011**, *41*(6), pp. 477–493. <https://doi.org/10.1016/j.jseaes.2011.01.019>.

36. Harris, R. A. The Nature of the Banda Arc – Continent Collision in the Timor Region. In *Arc-Continent Collision*; Brown, D.; Ryan, P. D., Eds.; Springer: Berlin, Heidelberg, Germany. **2011**; pp. 163–211. [https://doi.org/10.1007/978-3-540-88558-0\\_7](https://doi.org/10.1007/978-3-540-88558-0_7).
37. Tate, G. W.; McQuarrie, N.; Van Hinsbergen, D. J. J.; Bakker, R. R.; Harris, R.; Jiang, H. Australia Going Down Under: Quantifying Continental Subduction During Arc-Continent Accretion in Timor-Leste. *Geosphere*. **2015**, *11*, pp. 1860–1883. <https://doi.org/10.1130/GES01144.1>.
38. Audley-Charles, M. G. The Geology of Portuguese Timor. *Memoirs of the Geological Society of London*. **1968**, *4*, pp. 1–75.
39. Bachri, S.; Situmorang, R. L. Geological Research and Development Centre, Bandung, Indonesia, **1994**. *Geological Map of the Dili Quadrangle 2406-2407, East Timor, scale 1: 250.000*.
40. Partoyo, E.; Hermanto, B.; Bachri, S. Geological Research and Development Centre, Bandung, Indonesia, **1995**. *Geological Map of the Baucau Quadrangle 2057, East Timor, scale 1: 250.000*.
41. Boger, S. D.; Spelbrink, L. G.; Lee, R. I.; Sandiford, M.; Maas, R.; Woodhead, J. D. Isotopic (U-Pb, Nd) and Geochemical Constraints on the Origins of the Aileu and Gondwana Sequences of Timor. *Journal of Asian Earth Sciences*. **2017**, *134*, pp. 330–351. <https://doi.org/10.1016/j.jseaes.2016.11.026>.
42. Charlton, T. R.; Barber, A. J.; Harris, R. A.; Barkham, S. T.; Bird, P. R.; Archbold, N. W.; Morris, N. J.; Nicoll, R. S.; Owen, H. G.; Owens, R. M.; Sorauf, J. E.; Taylor, P. D.; Webster, G. D.; Whittaker, J. E. The Permian of Timor: Stratigraphy, Palaeontology and Palaeogeography. *Journal of Asian Earth Sciences*. **2002**, *20*, pp. 719–774.
43. Charlton, T. R.; Barber, A. J.; McGowan, A. J.; Nicoll, R. S.; Roniewicz, E.; Cook, S. E.; Barkham, S. T.; Bird, P. R. The Triassic of Timor: Lithostratigraphy, Chronostratigraphy and Palaeogeography. *Journal of Asian Earth Sciences*. **2009**, *36*, pp. 341–363. <https://doi.org/10.1016/j.jseaes.2009.06.004>.
44. Duffy, B.; Kalansky, J.; Bassett, K.; Harris, R.; Quigley, M.; van Hinsbergen, D. J. J.; Strachan, L. J.; Rosenthal, Y. Mélange Versus Forearc Contributions to Sedimentation and Uplift, During Rapid Denudation of a Young Banda Forearc-Continent Collisional Belt. *The Journal of Asian Earth Sciences*. **2017**, *138*, pp. 186–210. <https://doi.org/10.1016/j.jseaes.2017.02.008>.
45. Haig, D. W.; McCartain, E.; Mory, A. J.; Borges, G.; Davydov, V. I.; Dixon, M.; Ernst, A.; Groflin, S.; Håkansson, E.; Keep, M.; Santos, Z. Dos; Shi, G. R.; Soares, J. Postglacial Early Permian (late Sakmarian-early Artinskian) shallow-marine carbonate deposition along a 2000km transect from Timor to west Australia. *Palaeogeography, Palaeoclimatology, Palaeoecology*. **2014**, *409*, pp. 180–204. <https://doi.org/10.1016/j.palaeo.2014.05.009>.
46. Haig, D. W.; McCartain, E. Triassic Organic - Cemented Siliceous Agglutinated Foraminifera from Timor Leste: Conservative Development in Shallow - Marine Environments. *Journal of Foraminiferal Research*. **2010**, *40*, pp. 366–392.
47. Harris, R. A.; Sawyer, R. K.; Audley-Charles, M. G. Collisional Melange Development: Geologic Associations of Active Melange-Forming Processes with Exhumed Melange Facies in the Western Banda Orogen, Indonesia. *Tectonics*. **1998**, *17*, pp. 458–479.
48. Kenyon, C. S. Stratigraphy and Sedimentology of the Late Miocene to Quaternary Deposits of Timor. Doctor Thesis, University of London, London–England, **May 1974**.
49. Lisboa, J. V. V.; Silva, T. P.; De Oliveira D. P. S.; Carvalho, J. F. Mineralogical and Geochemistry Characteristics of the Bobonaro Melange of Western East Timor: Provenance Implications. *Comun. Geológicas*. **2020**, *106*, pp. 35–49. [https://www.lneg.pt/wp-content/uploads/2020/05/Volume\\_106.pdf](https://www.lneg.pt/wp-content/uploads/2020/05/Volume_106.pdf) (accessed on August 2021).
50. Park, S. I.; Kwon, S.; Kim, S. W. Evidence for the Jurassic Arc Volcanism of the Lolotoi complex, Timor: Tectonic Implications. *Journal of Asian Earth Sciences*. **2014**, *95*, pp. 254–265. <https://doi.org/10.1016/j.jseaes.2014.05.007>.
51. Standley, C. E.; Harris, R. Tectonic Evolution of Forearc Nappes of the Active Banda Arc - Continent Collision: Origin, Age, Metamorphic History and Structure of the Lolotoi Complex, East Timor. *Tectonophysics*. **2009**, *479*, pp. 66–94. <https://doi.org/10.1016/j.tecto.2009.01.034>.
52. Bird, P. An Updated Digital Model of Plate Boundaries. *Geochemistry, Geophysics, Geosystems* **2003**, *4*, pp. 1027–1080. <https://doi.org/10.1029/2001GC000252>.
53. Pisut, D. Plate Tectonic and Boundaries. **2020**. Available online: [https://services.arcgis.com/jIL9msH9OI208Gcb/arcgis/rest/services/Tectonic\\_Plates\\_and\\_Boundaries/FeatureServer](https://services.arcgis.com/jIL9msH9OI208Gcb/arcgis/rest/services/Tectonic_Plates_and_Boundaries/FeatureServer). (accessed on November 12, 2022).

54. Poiata, N.; Koketsu, K.; Miyake, H. Source Processes of the 2009 Irian Jaya, Indonesia, Earthquake Doublet. *Earth Planet Space*. **2010**, *62*, pp. 475–481. <https://doi.org/10.5047/eps.2010.02.008>.
55. Hale, M.; Plant, J. A. Introduction: The Foundation of Modern Drainage Geochemistry. In *Handbook of Exploration Geochemistry: Drainage Geochemistry*; Govett, G. J. S, Elsevier Science B.V; Amsterdam, Netherlands, **1994**; pp. 3–9.
56. Darnley, A. G.; Bjorklund, A.; Bolviken, B.; Gustavsson, N.; Koval, P. V.; Plant, J. A.; Steenfelt, A.; Tauchid, M.; Xuejing, X.; Garrett, R. G.; Hall, G. E. M. A Global Geochemical Reference Network & Field Methods for Regional Surveys. In *A Global Geochemical Database for Environmental and Resource Management: Recommendations for International Geochemical Mapping*; United Nations Educational, Scientific and Cultural Organization (UNESCO); Publishing House: Paris, France, **1995**; pp. 37–53.
57. Tanaka, T.; Kawabe, I.; Yamamoto, K.; Iwamori, H.; Hirahara, Y.; Mimura, K.; Asahara, Y.; Ito, T.; Yonezawa, C.; Dragusanu, C.; Kanda, S.; Shimizu, O.; Hayashi, M.; Miura, N.; Aoki, H.; Ohta, A.; Togami, K.; Toriumi, T.; Matsumura, Y.; Sakakibara, T.; Tanimizu, M.; Mizutani, Y.; Miyanaga, N.; Murayama, M.; Ohmori, F. Distributions of Elements in Stream Sediments in and around Seto City, Aichi Prefecture: An Attempt to a Geoenvironmental Assessment by Geochemical Mapping. *Geochemistry*. **1995**, *29*, pp. 113–125.
58. Fletcher, W. K. Stream Sediment Geochemistry in Today's Exploration World. In Proceedings of the Exploration 97: Fourth Decennial International Conference on Mineral Exploration, **1997**; pp 249–260.
59. Ohta, A.; Imai, N.; Terashima, S.; Tachibana, Y. Application of Multi-Element Statistical Analysis for Regional Geochemical Mapping in Central Japan. *Applied Geochemistry*. **2005**, *20*, pp. 1017–1037. <https://doi.org/10.1016/j.apgeochem.2004.12.005>.
60. Yamamoto, K.; Morishita, T. Preparation of Standard Composites for the Trace Elements Analysis by X-Ray Fluorescence. *Geological Society of Japan*. **1997**, *103*, pp. 1037–1045.
61. Balanda, K. P.; Macgillivray, H. L. Kurtosis: A Critical Review. *American Statistical Association*. **1988**, *42(2)*, pp. 111–119.
62. Dapples, E. C. Laws of Distribution Applied to Sand Sizes. *Geological Society of America*. **1975**, pp. 37–61.
63. De Carlo, L. T. On the Meaning and Use of Kurtosis. *American Psychological Association Inc.*. **1997**, *2(3)*, pp. 292–307.
64. Velasco, F.; Verma, S. P. Importance of Skewness and Kurtosis Statistical Tests for Outlier Detection and Elimination in Evaluation of Geochemical Reference Materials. *Mathematical Geology*. **1998**, *30(1)*, pp. 109–128.
65. Kurzl, H. Exploratory Data Analysis: Recent Advances for the Interpretation of Geochemical Data. *Journal of Geochemical Exploration*. **1988**, *30*, pp. 309–322.
66. Reimann, C.; Filzmoser, P.; Garrett, R. G.; Dutter, R. *Statistical Data Analysis Explained: Applied Environmental Statistics with R*, John Wiley & Sons: **2008**, 359 pp.
67. Reimann, C.; de Caritat, P. Establishing Geochemical Background Variation and Threshold Values for 59 Elements in Australian Surface Soil. *Science of the Total Environment*. **2017**, *578*, pp. 633–648. <https://doi.org/10.1016/j.scitotenv.2016.11.010>.
68. Sun, X.; Zheng, Y.; Wang, C.; Zhao, Z.; Geng, X. Identifying Geochemical Anomalies Associated with Sb-Au-Pb-Zn-Ag Mineralization in North Himalaya, Southern Tibet. *Ore Geology Reviews*. **2016**, *73*, pp. 1–12. <https://doi.org/10.1016/j.oregeorev.2015.10.020>.
69. Carranza, E. J. M. Exploratory Data Analysis. In *Encyclopedia of Mathematical Geosciences*; Sagar, B. S. D.; Cheng, Q.; McKinley, J.; Agterberg, F., Eds.; Springer, **1997**; pp. 364–368.
70. Howarth, R. J. *Dictionary of Mathematical Geosciences: with Historical Notes*, Springer: London, U.K., **2017**, 892 pp.
71. Zheng, Y.; Sun, X.; Gao, S.; Wang, C.; Zhao, Z.; Wu, S.; Li, J.; Wu, X. Analysis of Stream Sediment Data for Exploring the Zhunuo Porphyry Cu Deposit, Southern Tibet. *Journal of Geochemical Exploration*. **2014**, *143*, pp. 19–30. <https://doi.org/10.1016/j.gexplo.2014.02.012>.
72. Pan, G. Correlation Coefficient. In *Encyclopedia of Mathematical Geosciences*; Sagar, B. S. D.; Cheng, Q.; McKinley, J.; Agterberg, F., Eds.; Springer, **1997**; pp. 201–208.
73. Carranza, E. J. M.; Hale, M. A Catchment Basin Approach to the Analysis of Reconnaissance Geochemical-Geological Data from Albay Province, Philippines. *Journal of Geochemical Exploration*. **1997**, *60*, pp. 157–171.
74. Darwish, M. A. G. Stream Sediment Geochemical Patterns Around an Ancient Gold Mine in the Wadi El Quleib Area of the Allaqi Region, South Eastern Desert of Egypt: Implications for Mineral Exploration and

- Environmental Studies. *Journal of Geochemical Exploration*. **2017**, 175, pp. 156–175. <https://doi.org/10.1016/j.gexplo.2016.10.010>.
75. Demšar, U.; Harris, P.; Brunson, C.; Fotheringham, A. S.; McLoone, S. Principal Component Analysis on Spatial Data: An Overview. *Annals of the Association of American Geographers*. **2013**, 103, pp. 106–128. <https://doi.org/10.1080/00045608.2012.689236>.
  76. Kaiser, H. F. The Application of Electronic Computers to Factor Analysis. *Educational and Psychological Measurement*. **1960**, 20(1), pp. 141–151. <https://doi.org/10.1177/001316446002000116>.
  77. Panigrahi, N. Inverse Distance Weight. In *Encyclopedia of Mathematical Geosciences*; Sagar, B. S. D.; Cheng, Q.; McKinley, J.; Agterberg, F., Eds.; Springer, **1997**; pp. 666–672.
  78. Vilanova, V.; Ohtani, T.; Kojima, S.; Yatabe, K.; Cristovão, N.; Araujo, A. Modern River-Sand Geochemical Mapping in the Manufahi Municipality and Its Surroundings, Timor-Leste: Implications for Provenance. *MDPI Geosciences*. **2024**, 14, pp. 1–36. <https://doi.org/10.3390/geosciences14070177>.
  79. Kabata-Pendias, A.; Mukherjee, A. B. *Trace Elements from Soil to Human*, Springer-Verlag Berlin Heidelberg, **2007**, 561 pp.
  80. Winter, J. D. *Principles of Igneous and Metamorphic Petrology*, 2nd Ed.; Pearson Education Limited, London, U.K., **2007**, 561 pp.
  81. Wedepohl, K. H. *Handbook of Geochemistry*, Vol. II / 1-5; Springer-Verlag Berlin Heidelberg, **1978**.
  82. Greensmith, J. T. *Petrology of the Sedimentary Rocks*, 7th Ed.; UNWIN Hyman, London, U.K., **1988**, 271 pp.
  83. Zuffa, G. G. Unravelling Hinterland and Offshore Palaeogeography from Deep-water Arenites. In *Marine Clastic Sedimentology: Models and Case Studies (A Volume in Memory of C. Tarquin Teale)*; Leggett, J. K.; Zuffa, G. G., Eds.; Graham and Trotman: London, UK, **1987**, pp. 39–61.
  84. Tashakor, M.; Modabberi, S.; van der Ent, A.; Echevarria, G. Impacts of Ultramafic Outcrops in Peninsular Malaysia and Sabah on Soil and Water Quality. *Environmental Monitoring and Assessment*. **2018**, 190(6), pp. 1–19. <https://doi.org/10.1007/s10661-018-6668-5>.
  85. Vicente, V. A. S., Pratas, J. A. M. S., Santos, F. C. M., Silva, M. M. V. G., Favas, P. J. C., & Conde, L. E. N. Geochemical Anomalies from a Survey of Stream Sediments in the Maquelab Area (Oecusse, Timor-Leste) and Their Bearing on the Identification of Mafic - Ultramafic Chromite Rich Complex. *Applied Geochemistry* **2021**, 126. <https://doi.org/10.1016/j.apgeochem.2020.104868>.
  86. Kronberg, B. I.; Nesbitt, H. W.; Fyfe, W. S. Mobilities of Alkalis, Alkaline Earths and Halogens During Weathering. *Chemical Geology*. **1987**, 60, pp. 41–49.
  87. Nesbitt, W. H.; Markovics, G.; Price, R. C. Chemical Processes Affecting Alkalis and Alkaline Earths During Continental Weathering. *Geochimica et Cosmochimica Acta*. **1980**, 44, pp. 1659–1666.
  88. Ohta, A.; Minami, M. Less Impact of Limestone Bedrock on Elemental Concentrations in Stream Sediments- Case Study of Akiyoshi Area. *Bulletin of the Geological Survey of Japan*. **2013**, 64(6), pp. 121–138.
  89. Lapworth, D. J.; Knights, K. V.; Key, R. M.; Johnson, C. C.; Ayoade, E.; Adekanmi, M. A.; Arisekola, T. M.; Okunlola, O. A.; Backman, B.; Eklund, M.; Everett, P. A.; Lister, R. T.; Ridgway, J.; Watts, M. J.; Kemp, S. J.; Pitfield, P. E. J. Geochemical Mapping Using Stream Sediments in West-Central Nigeria: Implications for Environmental Studies and Mineral Exploration in West Africa. *Applied Geochemistry*. **2012**, 27(6), pp. 1035–1052. <https://doi.org/10.1016/j.apgeochem.2012.02.023>.
  90. Pirajno, F. *Hydrothermal Processes and Mineral Systems*; Springer Science and Business Media B. V., Perth, Australia, **2009**, 1273 pp.
  91. Silva-Filho, E. V.; Marques, E. D.; Vilaça, M.; Gomes, O. V. O.; Sanders, C. J.; Kutter, V. T. Distribution of Trace Metals in Stream Sediments Along the Trans-Amazonian Federal Highway, Pará State, Brazil. *Journal of South American Earth Sciences*. **2014**, 54, pp. 182–195. <https://doi.org/10.1016/j.jsames.2014.04.011>.
  92. Audley-Charles, M. G. The Geology of Portuguese Timor. Doctor Thesis, University of London, London-England; **1965**.
  93. Reimann, C.; Fabian, K.; Birke, M.; Filzmoser, P.; Demetriades, A.; Négrel, P.; Oorts, K.; Matschullat, J.; de Caritat, P.; The GEMAS Project Team. GEMAS: Establishing Geochemical Background and Threshold for 53 Chemical Elements in European Agricultural Soil. *Applied Geochemistry*. **2018**, 88, pp. 302–318. <https://doi.org/10.1016/j.apgeochem.2017.01.021>.
  94. Wang, M.; Hu, K.; Zhang, D.; Lai, J. Speciation and Spatial Distribution of Heavy Metals (Cu and Zn) in Wetland Soils of Poyang Lake (China) in Wet Seasons. *Society of Wetland Scientists*. **2019**, pp. 89–98. <https://doi.org/10.1007/s13157-017-0917-1/Published>.

95. Kierczak, J.; Pedziwiatr, A.; Waroszewski, J.; Modelska, M. Mobility of Ni, Cr and Co in Serpentine Soils Derived on Various Ultrabasic Bedrocks Under Temperate Climate. *Geoderma*. **2016**, *268*, pp. 78–91. <https://doi.org/10.1016/j.geoderma.2016.01.025>.
96. Dasgupta, S.; Roy, S.; Fukuoka, M. Depositional Models for Manganese Oxide and Carbonate Deposits of the Precambrian Sausar Group, India. *Economic Geology*. **1992**, *87*, pp. 1412–1418.
97. Gazley, M. F.; Collins, K. S.; Robertson, J.; Hines, B. R.; Fisher, L. A.; McFarlane, A. Application of Principal Component Analysis and Cluster Analysis to Mineral Exploration and Mine Geology. In AusIMM New Zealand Branch Annual Conference, **2015**; pp 131–139.
98. Ghezelbash, R.; Maghsoudi, A.; Daviran, M.; Yilmaz, H. Incorporation of principal component analysis, geostatistical interpolation approaches and frequency-space-based models for portraying the Cu-Au geochemical prospects in the Feizabad district, NW Iran. *Geochemistry*. **2019**, *79(2)*, pp. 323–336. <https://doi.org/10.1016/j.chemer.2019.05.005>.
99. Baldwin, G. J. Report of Activities 2016-17: Report ME 2017-001, Department of Natural Resources, Halifax, Nova Scotia, 2017. *Geoscience and Mines Branch*, pp 1–2. <https://doi.org/10.4095/248193>.

**Disclaimer/Publisher's Note:** The statements, opinions and data contained in all publications are solely those of the individual author(s) and contributor(s) and not of MDPI and/or the editor(s). MDPI and/or the editor(s) disclaim responsibility for any injury to people or property resulting from any ideas, methods, instructions or products referred to in the content.